Revision 1

The physical and chemical evolution of magmatic fluids in near-solidus silicic magma reservoirs: Implications for the formation of pegmatites

Juliana Troch[1,2], Chris Huber[1], Olivier Bachmann[3]

1 Department of Earth, Environmental and Planetary Sciences, Brown University, 324 Brook Street, Providence, RI 02912, USA

2 Department of Mineral Sciences, Smithsonian Institution National Museum of Natural History, 10th St & Constitution Avenue NW, Washington, DC 20560, USA

3 Institute of Geochemistry and Petrology, ETH Zürich, Clausiusstrasse 25, 8092 Zürich, Switzerland

To be submitted to American Mineralogist

Abstract

As ascending magmas undergo cooling and crystallization, water and fluid-mobile elements (e.g. Li, B, C, F, S, Cl) become increasingly enriched in the residual melt, until fluid saturation is reached. The consequential exsolution of a fluid phase dominated by H_2O (magmatic volatile phase or MVP) is predicted to occur early in the evolution of long-lived crystal-rich "mushy" magma reservoirs, and can be simulated by tracking the chemical and physical evolution of these reservoirs in thermomechanical numerical models. Pegmatites are commonly interpreted as the products of crystallization of late-stage volatile-rich liquids sourced from granitic igneous bodies. However, little is known about the timing and mechanism of extraction of pegmatitic liquids from their source. In this study, we review findings from thermomechanical models on the physical and chemical evolution of melt and MVP in near-solidus magma reservoirs, and apply these to textural and chemical observations from pegmatites. As an example, we use a three-phase compaction model of a section of a mushy reservoir, and couple this to fluid-melt and mineral-melt partition coefficients of volatiles trace elements (Li, Cl, S, F, B). We track various physical parameters of melt, crystals and MVP, such as volume fractions, densities, velocities, as well as the content in the volatile trace elements mentioned above. The results suggest that typical pegmatite-like compositions (i.e. enriched in incompatible elements) require high crystallinities (>70-75 vol% crystals) in the magma reservoir, at which MVP is efficiently trapped in the crystal network. Fluid-mobile trace elements can become enriched beyond contents expected from closed-system equilibrium crystallization

by transport of MVP from more evolved mush domains. From a thermomechanical perspective, these observations indicate that, rather than from melt, pegmatites may more likely be generated from pressurized, solute-rich MVP with high concentrations of dissolved silicate melt and fluid-mobile elements. Hydraulic fracturing provides a mechanism for the extraction and emplacement of such pegmatite-generating liquids in and around the main parental near-solidus mush as pockets, dikes, and small intrusive bodies. This thermomechanical framework for the extraction of MVP from mushes and associated formation of pegmatites integrates both igneous and hydrothermal realms into the concept of transcrustal magmatic distillation columns.

Keywords: magma reservoir, magmatic volatile phase, supercritical fluid, crystal mush, pegmatite, granite

Lexicon

Melt: a silicate-rich liquid with minor (<10 wt%) amounts of dissolved volatile species, such as H_2O, CO_2, Li, B, F, S, Cl, etc.

Fluid: H_2O-dominated phase that contains minor amounts of other components, such as fluid-mobile species and elements (CO_2 , Li, B, F, S, Cl, etc.) including those from dissolved rock-forming minerals (e.g. Si, Al, Na, K). A fluid can be liquid, gaseous/vaporous or supercritical in state.

Single-phase hydrous silicate liquid: a mixture of silicate melt and fluid at sufficiently high pressure and temperature to be above the critical curve and be completely miscible. No clear phase separations are expected between hydrous silicate liquid and fluid, and hydrous silicate liquid and melt, as these terms describe states in a continuous binary silicate-H2O system.

Magmatic Volatile Phase (MVP): a very general term for fluids and hydrous silicate liquids in magmatic systems

Brine: a saline fluid that forms when a fluid with dissolved salts separates into low-salinity vapor and high-salinity brine. The literature contains a wide range in terminology for these liquids, including hydrosaline liquid or melt, saline melt, chloride or salt melt.

1. Introduction

Over the last decades, our view of magma reservoirs has moved away from melt-dominated, vigorously convecting magma chambers (Shinohara and Hedenquist, 1997; Cloos, 2001) towards long-lived, crystal-dominated, mostly conductively-cooling magmatic systems (Bachmann and Bergantz, 2004; Hildreth, 2004; Marsh, 2004; Cooper and Kent, 2014; Bachmann and Huber, 2016; Cashman et al., 2017; Huber and Parmigiani, 2018; Jackson et al., 2018). More recently, advances in numerical methods have led to the development of increasingly complex thermo-mechanical models tracking the physical and chemical evolution of magma in these crystal-rich "mushy" reservoirs (e.g. Annen 2009, Degruyter and Huber 2014, Degruyter et al. 2019, Parmigiani et al. 2016, 2017). In particular, these models allow assessment of the effect of an exsolved magmatic volatile phase (MVP), which plays a key role in the chemical evolution and eruption behavior of magmatic systems (Wallace et al., 1995; Parfitt and Wilson, 2008; Degruyter et al., 2017; Cassidy et al., 2018; Townsend et al., 2019).

During magmatic differentiation, elements that are incompatible with the crystallizing mineral assemblage become increasingly enriched in the melt. Water behaves like an incompatible element and its concentration increases until reaching a solubility limit ("first boiling"), before further crystallization may then lead to continued water exsolution during "second boiling" (Frezzotti, 1992; Candela, 1994; Candela, 1997). Fluid-mobile trace elements (e.g. CO_2, Cl, S, Li, B, P, and noble gases) partition strongly into this typically H_2O-dominated fluid phase or MVP. As the solubility of water in the melt is strongly pressure-dependent (Burnham, 1967; Newman and Lowenstern, 2002; Liu et al., 2005; Papale et al., 2006 and references therein), most magmas stored in shallow magmatic systems reach MVP saturation early in their evolution (sometimes even at near-liquidus conditions for upper crustal arc settings).

Mechanically, this exsolved water-rich MVP migrates as positively-buoyant bubbles at low crystallinities (Fig. 1A). At intermediate crystallinities (~40 to 70 vol% crystals), the MVP forms connected channels (Fig. 1B), leading to the efficient removal of volatiles from the magma reservoir (Mungall, 2015; Oppenheimer et al., 2015; Parmigiani et al., 2016; Parmigiani et al., 2017; Lamy-Chappuis et al., 2020). At high crystallinities (>70 vol% crystals, Fig. 1C), the magmatic system becomes clogged with crystals, gas channels are obstructed, and MVP is trapped by capillary forces and cannot escape efficiently. Hence, as a magmatic system cools and approaches its solidus, MVP will accumulate and pressurize in the pore space of the mush.

Pegmatites are commonly interpreted as crystalline residues of late-stage volatile-rich derivatives of granitic magmas, and occur as exceptionally coarse-grained veins, pockets or large bodies (Niggli, 1912; Niggli, 1920; Cameron et al., 1949; Jahns and Tuttle, 1963; Norton, 1966; Jahns and Burnham, 1969; Thomas et al., 2000; London, 2018). They share both magmatic and hydrothermal characteristics as their bulk compositions approximate granitic minimum melts, they contain both melt and fluid inclusions, and

thermometry suggests formation temperatures of 400-600 °C. Aplites are often closely associated with pegmatites and could be regarded as their fine-grained cousins (Jahns and Burnham, 1969; Dill, 2015). Pegmatites are usually (but not always) associated with granitic source plutons (Shearer et al., 1992; Simmons and Webber, 2008). Such granitic plutonic bodies are increasingly recognized as residuals of magma reservoirs, which have either crystallized completely without erupting or which may have fed volcanic eruptions (Lipman, 1984; Bachmann et al., 2007; Deering and Bachmann, 2010; Laurent et al., 2020). In this paper, we review and evaluate models of pegmatite extraction from such source granites in light of current concepts in magma reservoir dynamics, in order to assess the physical properties of pegmatite-forming liquids, the magmatic processes involved in their formation and the timing of their formation in relation to the evolution of the magma reservoir. Rather than providing a definitive answer, we aim to build a bridge between the volcanic, plutonic, and pegmatitic research communities with the hope of initiating an integrated discussion of the processes bridging the magmatic and hydrothermal realms.

This integrative approach, both in concept and technique, was largely inspired by the philosophy and work of Jim Webster, the pioneer in the study of magmatic volatiles to whom this special issue and this paper are dedicated. Jim has provided the community with key observations on fluid-mobile elements and tools on how to track them in magmatic systems. His work has been an invaluable contribution to the scientific foundation that we have today, not only on the behavior of fluid-mobile elements in magmas, but also of their role in forming potentially exotic fluids. Perhaps most importantly, Jim's calm, positive and open-minded attitude has encouraged many, including us, to reach out between adjacent research communities, in the hope to further advance our understanding of these fascinating systems.

2. Background

2.1 Characteristics of pegmatites

The term "pegmatitic" is widely used to describe coarse-grained textures in a variety of rocks. In the stricter sense, however, "pegmatite" refers to broadly granitic intrusive bodies, pockets and dikes, which are characterized by spectacular coarse-grained textures and often contain minerals rich in fluid-mobile flux elements (Niggli, 1920; Barth, 1939; Jahns and Tuttle, 1963; London, 2009), e.g. spodumene, fluorite, apatite, tourmaline (Fig. 2) or Li- and F-bearing mica. Pegmatites are commonly associated with granitoid plutons, and although they can reach sizes of hundreds of meters, they are usually volumetrically small compared to these host plutons. Although only a minority of pegmatites are mineralized, they play an important role in our society, as zones can be enriched to economic values in

some of the rarest elements of our planet (Linnen et al., 2012; London and Kontak, 2012; Goodenough et al., 2019).

A key observation is that pegmatites usually do not erupt at the Earth's surface. While some rhyolitic lavas are extremely evolved and contain high concentrations of incompatible elements similar to those observed in pegmatites (e.g. Macusani rhyolite (Noble et al., 1984; London et al., 1988; Pichavant et al., 1988) or Taylor Creek rhyolite (Webster and Duffield, 1994)), these peraluminous magmas are typically hotter than pegmatites and are exceedingly rare compared to erupted volumes of "normal" metaluminous rhyolites.

Pegmatites are found in and around plutonic rocks of variable compositions (Beard and Day, 1986; Černý, 1991b; Černý, 1991a; Morton et al., 2018), but are more common in shallow, evolved silicic systems (producing "granitoids"), predominantly those that form either in collisional settings by partial melting of sediments (S-type granitoids) or in anorogenic environments (A-type granitoids). After many attempts to classify pegmatites, the most recent iteration has boiled down to two main families (Černý et al., 2005; Černý et al., 2012): (1) pegmatites enriched in lithium, cesium, and tantalum (LCT family), and (2) pegmatites enriched in niobium, yttrium, and fluorine (NYF family). These two families can often be directly linked to different source granitoids, with LCT pegmatites being spawned by S-type granites, while NYF pegmatites are usually related to A-type granitoids. The level of rare element enrichment in pegmatites often varies with distance from their source granitoids (Page, 1953; London, 2014).

Pegmatites display aspects of both igneous and hydrothermal systems (Jahns and Burnham, 1969; Nabelek et al., 2010; London and Kontak, 2012; Thomas and Davidson, 2013; Thomas and Davidson, 2016). On the one hand, they show a dominance of silicate minerals (quartz, feldspar, and mica), in proportions that approximate granitic whole-rock compositions (Stilling et al., 2006). On the other hand, massive quartz cores in many zoned pegmatites resemble hydrothermal quartz veins both in texture and composition (milky quartz with abundant fluid inclusions and low Ti and high Ge contents). Thermometry on pegmatites suggest that they formed at colder temperatures than even the most silicic magmas with temperatures <400-600 °C (Sirbescu and Nabelek, 2003; Anderson, 2012), significantly below the water-saturated haplogranitic solidus of ~650-680 °C (Johannes and Holtz, 1996). In line with this observation, pegmatites typically display the low-temperature polymorph of K-feldspar (microcline).

Other features of pegmatites are characteristic of neither magmatic nor hydrothermal systems, e.g. pegmatites often show strong enrichment in volatile and incompatible trace elements, such as B, Li, Nb, Ta, Sn, Be, REE, P, Rb, Cs, U, and Th compared to most magmas and hydrothermal fluids, resulting in unusual mineralogy (e.g. Fig. 2, Morton et al., 2018). Additionally, many pegmatites exhibit pronounced textural and compositional zoning, with typically finer-grained outer zones, monomineralic layering and

inward crystal coarsening that may produce up to meter-sized crystals in the center (Cameron et al., 1949). Pegmatites typically lack developed thermal contact aureoles around them (Anderson, 2012), and thermal models suggest that they cool in hours to days in an upper crustal environment (Chakoumakos and Lumpkin, 1990). Their bulk-rock composition is extremely difficult to constrain (Sánchez-Muñoz et al., 2017), as grain-sizes are typically very large and modal variations abrupt. Moreover, intensive re-crystallization and overprinting by late high- and low-temperature fluids occur in many pegmatites (e.g. REE remobilization by fluids at Strange Lake, Gysi et al., 2016). Some pegmatites demonstrate low emplacement pressure through the presence of large miarolitic cavities (Fig. 2B), while others have lost any residual porosity, and potentially suggest deeper emplacement (Schaltegger et al., 2015).

2.3 Models for pegmatite formation

Models for pegmatites agree that two ingredients play a key role in their origin: (1) water- and/or volatile-rich melt of broadly granitic composition, and (2) flux elements, such as F, B, and P, which lower the solidus and lead to depolymerization of the melt. Below, we summarize the key aspects of several models for pegmatite formation. The difference between these contrasting models boils down to the question of whether the concentration in water, flux and incompatible elements is a local, microscopic phenomenon at mineral boundaries during crystallization from an otherwise "typical" granitic melt, or whether this accumulation is more general, potentially leading to somewhat exotic hydrous silicate liquids that are neither granitic melts nor aqueous fluids. This paper focuses on pegmatites derived from granitic source plutons, however, we note that some pegmatites (mostly LCT) cannot clearly be linked to such plutons and are thought to have formed by crustal anatexis (Kontak and Kyser, 2009; Müller et al., 2017; Fuchsloch et al., 2018; Ashworth et al., 2020). We stress here that the physical processes that we later invoke for the extraction of pegmatite-forming liquid from its source are independent of the size or the origin of the reservoir from crustal anatexis or mantle-derived magmas.

Model 1: Precipitation from hydrous melt and magmatic fluids

The kinship between pegmatites and both magmatic and hydrothermal rocks has been recognized for more than a century, and early works emphasize the importance of magmatic volatile elements ("gaseous mineralizators", Niggli, 1912) in the formation of pegmatites (Niggli, 1920; Barth, 1939). About 50 years ago, in a now classical study, Jahns and Burnham (1969) highlight the role of water and other volatile elements, such as alkalis, "lithia and other hyperfusible elements". They describe pegmatite formation as a three-step closed-system process at the magmatic-hydrothermal transition, beginning with crystallization of a hydrous silicate melt, transitioning to concomitant crystallization from silicate melt

and an exsolved supercritical aqueous fluid, and ending with crystallization from aqueous fluid in the absence of melt (Jahns and Burnham, 1969). Although they admit that element and mineral solubilities in the fluid are limited, they suggest that an aqueous phase could be a "powerful scouring agent" for extracting and transporting elements from the melt, due to its ability to move easily relative to highly-viscous silicate melt.

Model 2: Crystallization from undercooled silicate melt

A second model puts more emphasis on the role of silicate melt and common textures in granitic pegmatites, including monomineralic zonation and layering, graphic intergrowth, and giant crystal growth. Based on kinetic cooling experiments, undercooling of low-diffusivity, high-viscosity silicate melt has been suggested to play a major role in producing these typical pegmatite textures (London, 2008; London, 2009; London, 2014). During this forced disequilibrium crystallization, incompatible elements, including flux elements like H_2O, F, B, Li etc., become enriched in a boundary layer at the growth front of the crystal, leading to locally lower viscosities (Bartels et al., 2011; Bartels et al., 2013) and increased diffusivity and replenishment of mineral-forming elements, which results in increased and rapid crystal growth (London, 2009). In such highly-fluxed silicate melt, nucleation of minerals is delayed, and melt can survive at temperatures below the granitic solidus (Sirbescu and Nabelek, 2003; Nabelek et al., 2010; London, 2014; Sirbescu et al., 2017). Water saturation is considered neither necessary nor likely by some authors (London, 1992).

Model 3: Precipitation from single-phase hydrous silicate liquid

It has long been recognized that with higher pressures and temperatures, H_2O-dominated fluids and silicate melts become increasingly miscible (Bureau and Keppler, 1999; Ni et al., 2017), forming a single-phase hydrous silicate liquid at supercritical conditions (Fig. 3). Water solubility in silicate melt and thus miscibility between silicate melt and MVP is enhanced for strongly depolymerized melts (Mysen, 2007), and therefore greatly depends on melt composition. Several elements have been identified as strong network modifiers, which lead to depolymerization of the silicate melt network and thus to increased water solubility: Fluorine (Sowerby and Keppler, 2002; Giordano et al., 2004; Mysen et al., 2004; Bartels et al., 2013), boron (Pichavant, 1987; Sowerby and Keppler, 2002) and alkali elements such as Na, Li, K, Rb and Cs (Franz and Scholze, 1963; Mesko and Shelby, 2001; Mesko et al., 2002; Sowerby and Keppler, 2002; Rapp and Shelby, 2003). Hydrous silicate liquids with high concentrations of these elements are inferred to have low viscosities (Nabelek et al., 2010; Bartels et al., 2011; Thomas and Davidson, 2012), and are used in industrial applications under the term "geopolymers" (Davidovits, 1991;

This is the peer-reviewed, final accepted version for American Mineralogist, published by the Mineralogical Society of America.
The published version is subject to change. Cite as Authors (Year) Title. American Mineralogist, in press.
DOI: https://doi.org/10.2138/am-2021-7915. http://www.minsocam.org/

MacKenzie, 2006; Nair et al., 2007). Based on melt inclusions in several pegmatitic systems, it has been suggested that pegmatites form from such flux-rich single-phase hydrous silicate liquids (Thomas et al., 2000; Thomas et al., 2006; Thomas and Davidson, 2012; Thomas et al., 2012; Thomas and Davidson, 2013; Thomas and Davidson, 2016; Thomas et al., 2019). However, it remains yet unclear how volumetrically significant such single-phase liquids are in magmatic systems, and whether some of these inclusions may represent mixed inclusions of co-entrapped fluid and silicate melt rather than a supercritical liquid (Fiedrich et al., 2020a).

3. Methods for simulating near-solidus magma reservoirs

The formation and chemical makeup of pegmatites are tied to the evolution of near-solidus magma bodies, which is controlled by both physical-mechanical and chemical processes among the three phases crystals, melt and MVP. In this section, we describe two complementary models: (1) a three-phase compaction model (crystals, melt, and MVP), which focuses on the mechanical interaction between these phases in a deforming crystal-rich mushy magma, and (2) a simple mass-balance model for variably fluid-mobile trace elements, which tracks their enrichment in a crystallizing mush in which MVP migrates from deeper, more crystal-rich zones and accumulates in shallower and more melt-rich horizons (Parmigiani et al., 2016).

3.1 Simulation A: Three-phase compaction in silicic magma reservoirs

The three-phase compaction simulation tracks the distribution of crystals, melt, and MVP in a subsection of a crystal-rich mush system. Over time, these phases will re-distribute driven by their contrast in density. The simulation solves for the mass and momentum conservation of a crystalline matrix, melt and MVP, which are coupled through drag terms, interfacial tension, and phase changes. These equations are complemented by an energy conservation statement that relates the pressure differences between the different phases with compaction. The simulation is based on the three-phase compaction model in Huber and Parmigiani (2018), with some slight changes to the governing equations. Table 1 lists the symbols used in the following equations, their units and the values chosen in the simulations. The contrast in viscosity between minerals, melt and MVP allows us to neglect shear stresses in the MVP. Mass conservation in a crystallizing and degassing mush follows

$$\frac{\partial(1-\phi)}{\partial t} + \frac{\partial\left(V_x(1-\phi)\right)}{\partial z} = \frac{\Gamma_x}{\rho_x} \quad (1)$$

$$\frac{\partial\phi(1-S)}{\partial t} + \frac{\partial\left(V_m(1-\phi)\right)}{\partial z} = \frac{\Gamma_f}{\rho_m} - \frac{\Gamma_x}{\rho_m} \quad (2)$$

This is the peer-reviewed, final accepted version for American Mineralogist, published by the Mineralogical Society of America.
The published version is subject to change. Cite as Authors (Year) Title. American Mineralogist, in press.
DOI: https://doi.org/10.2138/am-2021-7915. http://www.minsocam.org/

$$\frac{\partial\left(\rho_x V_x(1-\phi)+\rho_m V_m \phi(1-S)+\rho_f V_f \phi S\right)}{\partial z} = 0 \quad (3)$$

where Eqns. 1 and 2 describe mass conservation for the crystal and melt phases respectively, and Eqn. 3 is a statement of total (all three phases) mass conservation. In these equations, ϕ refers to the porosity or volume fraction taken up by melt and MVP, and S is the pore volume fraction occupied by the MVP. The variables Γ_x and Γ_f are phase change terms describing the rate of crystallization and exsolution, and V is the velocity for either of the three phases (index x = crystals, m = melt and f = MVP). These equations are complemented by a momentum conservation equation for each phase

$$0 = -(1-\phi)\left[\frac{\partial P_x}{\partial z} - \rho_x g\right] + \left(P_x - P_f\right)\frac{\partial \phi}{\partial z} + \frac{4}{3}\frac{\partial}{\partial z}\left[(1-\phi)\mu_x \frac{\partial V_x}{\partial z}\right] - c_1(V_x - V_m) \quad (4)$$

$$0 = -\phi(1-S)\left[\frac{\partial P_m}{\partial z} - \rho_m g\right] + \left(P_m - P_f\right)\frac{\partial \phi S}{\partial z} + \frac{4}{3}\frac{\partial}{\partial z}\left[\phi(1-S)\mu_m \frac{\partial V_m}{\partial z}\right] + c_1(V_x - V_m) - c_2\left(V_m - V_f\right) \quad (5)$$

$$0 = -\phi S\left[\frac{\partial P_f}{\partial z} - \rho_f g\right] + c_2\left(V_m - V_f\right) \quad (6)$$

where μ is the viscosity of matrix, melt or MVP (for indices x, m, and f, respectively), c_1, c_2 are drag coefficients that include the relative permeabilities of the medium and the viscosity of the different phases (Huber and Parmigiani, 2018) and P refers to the pressure in each phase.

Finally, energy conservation statements for the melt-crystal and melt-MVP interfaces (Huber and Parmigiani, 2018) give

$$P_x - P_m = -\frac{K_0 \mu_x}{\phi(1-\phi)}\left[\frac{\partial \phi}{\partial t} + V_x \frac{\partial \phi}{\partial z}\right] + \Gamma_x\left[\frac{P_m}{\rho_m} - \frac{P_x}{\rho_x} + L_x\right] \quad (7)$$

$$P_m - P_f = -\frac{K_0' \mu_m}{\phi^2 S(1-\phi)}\left[\frac{\partial \phi S}{\partial t} + V_m \frac{\partial \phi S}{\partial z}\right] + \Gamma_f\left[\frac{P_m}{\rho_m} - \frac{P_f}{\rho_f} + L_f\right] \quad (8)$$

In Eqns. 7 and 8, variables α_1 and α_2 are interfacial densities (crystal-melt and melt-MVP), σ_1 and σ_2 are the crystal-melt and melt-MVP interfacial tensions, K_0 and K_0' are geometric factors (Bercovici et al., 2001), and L_x and L_f are the latent heat of crystallization and exsolution. While the crystallization rate Γ_x is fixed in the following calculations, MVP exsolution is computed from water mass-balance. Closure equations including material properties are set similarly to Huber and Parmigiani (2018). In all calculations, the mush is assumed to have a thickness of 20 m and therefore can be regarded as a smaller subset of a larger mushy system. Each phase is initially homogenously distributed with ϕ=0.45 and S=0.15. The calculations are ended when the melt fraction ϕ(1-S) reaches a local minimum of 0.03. We neglect supercritical MVP compressibility due to its limited variability over the investigated depth interval of 20 m.

This is the peer-reviewed, final accepted version for American Mineralogist, published by the Mineralogical Society of America.
The published version is subject to change. Cite as Authors (Year) Title. American Mineralogist, in press.
DOI: https://doi.org/10.2138/am-2021-7915. http://www.minsocam.org/

3.2 Simulation B: Theoretical Determination of Upward Disequilibrium Enrichment (TheDUDE)

As a baseline for the behavior of incompatible trace elements in a crystallizing magmatic system, we use the simple mass balance equation for closed-system equilibrium or batch crystallization (Schilling, 1966)

$$C_M = \frac{C_0}{\phi(1-S)+ K_D^x(1-\phi(1-S))} \quad (9)$$

where C_M is the concentration of a trace element in the melt, C_0 is the initial concentration of that element, $\phi(1\text{-}S)$ is the melt fraction and K_D^x the distribution coefficient for an element x between melt and the bulk mineral assemblage.

The density contrast between the three phases ($\rho_x > \rho_m > \rho_f$) and pressure changes caused by phase changes provide the mechanical energy required to redistribute the phases over time, which may affect the distribution of trace elements if these phases are not fully chemically equilibrated. Based on the results from the mechanical simulations in Simulation A (section 3.1), we develop a simple mass-balance model for the distribution of volatile trace elements and their transport in the MVP. Typical diffusion coefficients of some Fluid-mobile elements in silicic melts are sufficiently small (e.g. about 10^{-12} m^2/s for Cl and F at near-solidus temperatures (Watson, 1991; Bai and van Groos, 1994; Gabitov et al., 2005)) that the rapid migration of MVP may prevent diffusive re-equilibration between melt and MVP during MVP ascent from the compacting (bottom) to the decompacting (top) region of a maturing mush. For simplicity, we assume that within mature and dynamically compacting mushes, trace element distribution among the three phases remains close to equilibrium in a closed system with limited MVP transport. Disequilibrium trace element transport via a migrating MVP begins when crystallinity and degree of compaction are large enough to have established a well-developed decompaction layer with MVP accumulation at the top.

The Theoretical Determination of Upward Disequilibrium Enrichment (or TheDUDE simulation) assumes that the deeper section of the compacting mush and the top layer evolve (chemically) independently (no transport between them) until the crystallinity of the mush and pore volume fraction of MVP are large enough to allow for sufficiently high MVP migration rates (Huber et al., 2012; Parmigiani et al., 2016). We assume that the bottom section of the mush (index b) evolves as a closed system and under equilibrium conditions to a porosity ϕ^b and MVP pore volume fraction S^b. Independently, the decompacting top portion of the mush (index t) reaches a porosity ϕ^t and MVP pore volume fraction S^t also under closed and equilibrium conditions. When conditions for MVP transport as simulated by Simulation A are reached, MVP from the bottom layer is able to invade the top layer and mix with it, so that the MVP pore volume fraction evolves as $S^{t'}=S^t+\Delta S$, where ΔS is the MVP fraction added by the upward transport. Based on the higher rate of diffusive exchange between MVP and melt compared to

slow diffusive equilibration between melt and crystals, we assume that the melt at the top of the mush has fully equilibrated chemically with the new MVP mixture, but not with the surrounding minerals. We then compute the maximum degree of enrichment of volatile trace elements in the melt in the top layer compared to the bottom layer.

After some algebra, we can find a parameterization for the degree of enrichment possible by transport of MVP coming from deeper, more fractionated parts of the system

$$\frac{C_x^t}{C_m^{t\prime}} = K_{x-m}\left[1 + \frac{K_{f-m}(\psi_1 - 1)}{(S^t + \Delta S^t)K_{f-m} + (1 - S^t - \Delta S^t)}\right]^{-1} \quad (10)$$

where the ratio of trace element enrichment at the top versus the bottom of the mush (ψ_1) is defined as

$$\psi_1 = \frac{\rho_x(1-\phi^t)K_{x-m} + \rho_m\phi^t(1-S^t) + \rho_g\phi^t S^t K_{f-m}}{\rho_x(1-\phi^b)K_{x-m} + \rho_m\phi^b(1-S^b) + \rho_g\phi^b S^b K_{f-m}} \quad (11)$$

Finally, $\bar{\rho}^t$ and $\bar{\rho}^b$ are the average densities of the magma at the top and bottom layers, with

$$\bar{\rho}^t = (1-\phi^t)\rho_x + \phi^t(1-S^t)\rho_m + \phi^t S^t \rho_g \quad (12)$$

and $K_{x\text{-}m}$ and $K_{f\text{-}m}$ are the partition coefficients between minerals and melt and MVP and melt respectively for the trace element of interest.

4. Results

4.1 Simulation A: Observed physical changes

The objective of the simulation is to tie crystallization to the exsolution of the MVP and illustrate how density and viscosity differences among phases drive migration and accumulation of MVP in shallow decompacting lenses at the top of the magma body. In the simulated mush section, compaction leads to heterogeneous phase distribution and a decompacting layer is rapidly established at the top of the mush, resulting from the accumulation of MVP (Fig. 4A+B). As crystallization and exsolution proceed, the crystal volume fraction in this layer decreases and the MVP volume fraction increases (Fig. 4A+B), because melt and crystals are continuously displaced downwards by the MVP. As a result, the decompacting layer grows in thickness over time (Fig. 4B), until it is volumetrically dominated by MVP. The velocity of rising MVP increases linearly during its ascent, reaching a maximum right before joining the decompacting layer (Fig. 4C). Over time, the velocity contrast increases as a function of the increasing density contrast between the well-established compacting and decompacting layers (Fig. 4C). This mechanical modeling illustrates how the transfer of MVP from deeper crystal-rich sections of a mush becomes efficient once compaction has developed significant crystallinity contrast across the mush, as can be expected for a mature, mushy magma reservoir.

This is the peer-reviewed, final accepted version for American Mineralogist, published by the Mineralogical Society of America.
The published version is subject to change. Cite as Authors (Year) Title. American Mineralogist, in press.
DOI: https://doi.org/10.2138/am-2021-7915. http://www.minsocam.org/

334

335 **4.2 Simulation B: Chemical evolution**

336 Closed-system equilibrium or batch crystallization suggests that water and incompatible element increase
337 exponentially in melt and MVP with increasing crystal volume fraction, and therefore most enrichment
338 occurs at extremely high crystallinities (Fig. 1E+F). This is particularly apparent in cases where water is
339 efficiently purged from the system at intermediate crystallinities (Fig. 1D+E). As can be expected,
340 enrichment of water and incompatible elements is further promoted by initially higher concentrations and
341 high degrees of incompatibility. Overall, it suggests that during near-complete crystallization, trace
342 element enrichment in the melt by more than a factor of 10 can only occur for the most incompatible
343 elements (K_D <0.05).

344 In order to assess the potential for trace elements dissolved in MVP to equilibrate with the surrounding
345 mush during MVP transport, we calculate the Péclet number for five volatile elements with different
346 diffusivities: Boron with $D_B \approx 10^{-15}$ m/s (Mungall et al., 1999), sulfur with $D_S \approx 10^{-13}$ m/s (Watson, 1994;
347 Lierenfeld et al., 2018), chlorine with $D_{Cl} \approx 10^{-12}$ m/s (Watson, 1991; Bai and van Groos, 1994), fluorine
348 with $D_F \approx 10^{-11}$ m/s (Gabitov et al., 2005), and lithium with $D_{Li} \approx 10^{-9}$ m/s (Holycross et al., 2018). The
349 Péclet number is defined as

350 $$Pe = v \frac{d}{D_x} \quad (13)$$

351 where v is the velocity of MVP, d the pore diameter (estimated here to be around 100 µm based on the
352 characteristic diffusion distance (Huber et al., 2012)), and D_x the diffusivity of the element x. A value of
353 Pe > 1 indicates MVP transport on much faster timescales than element transport through diffusion
354 (Huber et al., 2012), greatly limiting the ability for MVP and melt to chemically equilibrate. For $v < 10^{-12}$
355 m/s, MVP is likely equilibrated completely, with Pe << 1 for all elements. For $v > 10^{-7}$ m/s (similar to
356 highest velocity modelled in Fig. 4C), Pe ≥ 1 for all elements, except the extremely fast-diffusing Li.
357 Already for the lowest MVP upward velocity shown in Fig. 4C, equilibration is limited for most volatile
358 elements.

359 Tracking trace element concentrations via our trace element enrichment simulation (see section 3.2)
360 shows in greater detail how at high crystal contents (~0.7-0.8), MVP is transported rapidly enough
361 through the mush that it is not able to fully re-equilibrate with surrounding melt and crystals during its
362 ascent from deeper more fractionated horizons to the accumulation zone at the top. The result is a
363 significant enrichment in fluid-mobile trace elements, which we have calculated as examples for the
364 elements in Fig. 5 using partition coefficients listed in Table 2. Enrichment of trace elements in the
365 decompacting top layer compared to the compacting bottom layer is favored by a number of factors,

mainly the amount of MVP added to the top layer, large contrasts in porosity and MVP volume fraction between top and bottom layer, as well as high fluid-melt and melt-crystal partition coefficients (Fig. 5). The order by which any volatile trace element becomes enriched is controlled by its partitioning behavior between the melt and the bulk mineral assemblage (here a roughly eutectic assemblage of 1/3 quartz + 1/3 plagioclase + 1/3 sanidine), and its fluid-melt partition coefficient. In systems with large contrasts in porosity or crystallinity between the compacting and decompacting regions (Fig. 5A), the order by which trace elements become enriched is predominantly controlled by their crystal-melt partition coefficients (here S < B < Cl = Li < F, Table 2). We note that crystal-melt partitioning data for these volatile elements is very limited for silicic systems (Table 2), and it is likely that some elements, such as F, are more incompatible than shown by this model. In systems with less porosity contrast but larger difference in MVP pore volume fraction (Fig. 5B), it is primarily the fluid-melt partition coefficient that controls the order by which trace elements become enriched in the decompacting top layer (here S > Cl > B > Li > F, Table 2). The amount of MVP amplifies the differences in concentration of these different elements (Fig. 5C). Under favorable conditions, this disequilibrium enrichment in trace elements through the flushing of MVP can increase the concentrations of incompatible elements by a factor of 10 or more relative to closed-system fractional crystallization (Fig. 5).

5. Discussion

Our results demonstrate how physical processes such as phase separation and compaction control the composition of melt and MVP in upper-crustal silicic magma reservoirs. Due to its mobile nature compared to the slow transport of melt and crystals, MVP plays a particularly important role in the differentiation and enrichment of magmas in incompatible elements, particularly in those that are fluid-mobile. In the following section, we will discuss how these mechanisms could be linked to specific models of pegmatite formation, and how an integrated view of pegmatites and crystal-rich "mushy" magma reservoirs stored at near-solidus conditions over long timescales could solve (some of) the issues summarized as the "pegmatite puzzle" by London and Morgan (2012):

1. When and how are pegmatites derived from their host granite?
2. How do pegmatites acquire their increasing chemical fractionation from the source?
3. When in their history do granites becomes saturated with MVP, and how do pegmatites relate to this magmatic-hydrothermal transition?

5.1 Enrichment in incompatible elements

Volcanic eruptions require efficient extraction of melt from the mushy host magma reservoir, which is limited to crystal volume fractions below the 50 % considered as the rheological lockup threshold (Marsh, 1981; Vigneresse et al., 1996; Dufek and Bachmann, 2010). Rather than for extraction of rare elements, juvenile volcanic deposits are, if at all, mined as abrasives, for products in the construction industry, or for soil improvement (e.g. Austin, 1994; Troll et al., 2017). These observations indicate that pegmatites are generally more enriched in incompatible elements than most rhyolites, suggesting that the source region for pegmatitic liquids may be fundamentally different in composition and degree of differentiation compared to the state of the source region for most silicic volcanic eruptions.

During the magmatic evolution, differentiation by equilibrium and fractional crystallization leads to the continuous enrichment in incompatible elements and water in the melt. Equilibrium and fractional crystallization both imply that trace element enrichment is exponential (Fig. 1), suggesting that enrichment is limited in the early stages of the magmatic evolution, in which magma is still mobile and could be extracted for volcanic eruptions. Enrichment increases by orders of magnitude at 80-90 vol% crystallization, when MVP and melt are effectively trapped in the crystal framework. This is relatively independent of whether trace element enrichment occurs due to equilibrium/batch crystallization or due to fractional/Rayleigh crystallization, with the difference between them being negligible until ~60-70 vol% crystals (Fig. 1). Additional input of MVP into these regions can increase the concentrations of fluid-mobile trace elements beyond what is expected for closed-system equilibrium (section 4.2, Fig. 5). For pegmatites, their low-temperature origin, extremely evolved compositions, and strong enrichment in incompatible elements up to economic concentrations (section 2.2) indicate that they are sourced from highly fractionated, crystal-rich magmatic environments.

5.2 Volatile saturation and timing of pegmatite formation

The presence of a MVP is commonly predicted in recently developed models of mush-dominated magma reservoirs (Edmonds and Wallace, 2017; Parmigiani et al., 2017; Degruyter et al., 2019) and is fundamental in controlling differentiation processes and, in some cases, explosivity in magmatic systems (Anderson et al., 1984; Sisson and Bacon, 1999; Pistone et al., 2015; Degruyter et al., 2017; Bachmann and Huber, 2018; Cassidy et al., 2018; Popa et al., 2019). Decades of careful work describing solubilities and H_2O-CO_2 concentrations in magmas (Tuttle and Bowen, 1958; Burnham and Jahns, 1962; Dingwell et al., 1984; Holtz et al., 1992; Newman and Lowenstern, 2002; Papale et al., 2006) or tracking exsolution through fluid-mobile trace elements (Webster and Rebbert, 1998; Webster et al., 2020) provide a clear answer to the question of when volatile saturation occurs in a magmatic system's history; intermediate to silicic mushes in the mid to upper crust will become saturated with a MVP starting at low crystal volume

fractions. In arc systems, it is likely that magmas become saturated near their liquidus temperature during their ascent through the upper crust, and even the driest magmas (and mafic magmas) will eventually become saturated with a fluid phase as crystallinities reach >80-90 vol%.

As illustrated by our compaction model (section 4.1), mushy crystal-rich magma reservoirs contain plenty of high-crystallinity source regions that could produce liquids with pegmatite-type trace element enrichments (Fig. 1F), but most of these regions see accumulation of MVP rather than of melt (Fig. 1E). If pegmatites were sourced from mushy near-solidus magma reservoirs, as their evolved character and low temperatures indicate, it would be more likely for them to form from volumetrically dominant MVP. At these conditions, rhyolitic/granitic melt is present in extremely small volumes, which are finely disseminated throughout the host mush. The limited density contrast between the melt and the granitic mineral assemblage of quartz and feldspars coupled to the relatively high viscosity even of water-saturated rhyolite melt make it very unlikely that large enough volumes of crystal-free melt could accumulate and be extracted to form pegmatites at the suggested pegmatite formation timescales of days to months (Chakoumakos and Lumpkin, 1990; Morgan and London, 1999; Webber et al., 1999).

As crystallinity increases beyond ~70 vol%, capillary forces become dominant, trapping MVP and highly-evolved melt into the crystal mush framework (Parmigiani et al., 2016; Parmigiani et al., 2017; Lamy-Chappuis et al., 2020). Exsolution will drive overpressurization and cause episodic hydraulic fracturing (Fig. 1C, Holtzman et al., 2012) or release solitary waves (Connolly, 2010). These events could send pulses of supercritical MVP and small amounts of silicate melt into cracks within the borders of the dying mushy reservoirs. The implication for episodic rapid transport of otherwise static MVP in the context of long-lived mush reservoirs in the crust with slow phase separation (Marsh, 1981; Koyaguchi and Kaneko, 1999; Huber et al., 2009; Bachmann and Huber, 2018) is that there is sufficient time for magmas to equilibrate with an exsolved MVP before it is expelled. The MVP therefore likely contains abundant dissolved melt components, such as the silica and alkali elements suggested by pegmatite models favoring an origin from single-phase hydrous silicate liquids (section 2.3). Precipitation of minerals from this MVP could lead to the typical quartz- and feldspar-dominated pegmatite assemblages. Hydraulic fracturing provides both a physical mechanism and an explanation for the timing of pegmatite formation in the context of the evolution of a magmatic reservoir. It could also explain the common occurrence of pegmatites as veins, dikes or larger bodies, which tend to be structurally controlled and exploit regional zones of weakness in the crust (Brisbin, 1986).

5.3 Granitic source flavors and element solubility

463 It has long been recognized that pegmatites occur primarily in association with S- and A-type granites,
464 with the two main groups, LCT- and NYF-pegmatites, directly linked to these different granite families.
465 In contrast, the voluminous, typically water-rich I-type granitoids generally related to subduction zones
466 seem to produce few large and mineralized pegmatite bodies. Instead, they show abundant quartz veins,
467 commonly source volcanic eruptions, and sometimes develop large porphyry ore deposits (Sillitoe, 2010;
468 Černý et al., 2012). This difference may be a consequence of two main processes: (1) Compositional
469 differences and their effect on water and element solubility, and (2) differences in water concentrations
470 resulting in MVP saturation at different stages of crystallization.
471 First, S- and A-type magmas appear enriched in key flux elements (such as Li, B, F, P) in comparison to
472 I-type magmas (Whalen et al., 1987; Taylor and Fallick, 1997; Trumbull et al., 2008). As recognized in
473 models favoring pegmatite formation from single-phase hydrous silicate liquid (section 2.3), these flux
474 elements generally partition into the fluid phase (Webster et al., 1989; Zajacz et al., 2008; Iveson et al.,
475 2019), increase the ionic potential of the fluid, and can thus lead to the progressive dissolution of other,
476 typically less soluble, cations (e.g., Si, Al, Na, K, Zr, and REE). In I-type magmatic systems, silicate melt
477 and MVP may therefore be less prone to reaching miscibility, and melt and MVP remain more dissimilar
478 to one another compared to A- and S-type granitic systems. Exsolved MVP in I-type systems may more
479 closely resemble classical S- and Cl-bearing hydrothermal fluids and brines involved in the generation of
480 quartz veins and S-rich ore deposits (e.g. porphyry copper deposits).
481 Second, arc magmas typically reach water-saturation early in their evolution, while many A- and S-type
482 granites show evidence of a protracted evolution at H_2O-undersaturated conditions (Huang and Wyllie,
483 1981; Bartoli et al., 2013). With MVP outgassing being most efficient at intermediate crystallinities (Fig.
484 1), the MVP can be expected to be more efficiently purged before I-type systems reach enriched melt
485 compositions. The early exsolution of MVP could effectively flush out the fluid-mobile flux elements
486 required to enhance element solubility in the MVP and water solubility in the melt. To a first order, our
487 trace element model (section 4.2) illustrates how differences in crystallinity and MVP pore volume
488 fraction can lead to and manifest compositional differences between I-type and S- and A-type magmatic
489 systems (Fig. 5). Here, accumulation of S and Cl is particularly efficient in MVP-dominated systems at
490 intermediate crystallinities and small porosity differences, which would more closely resemble I-type
491 systems. Accumulation and removal of S from such systems may also be enhanced by the dependence of
492 K_D^S on fO_2 (e.g. Scaillet et al., 1998), leading to high fluid-melt partition coefficients in oxidizing I-type
493 systems. Coupling of trace element distributions to physical models via experimentally-derived partition
494 coefficients may therefore prove to be a powerful tool for tracking the crystallization and degassing
495 history of magma reservoirs in the future.

Traditionally, major element solubilities in aqueous fluids are considered to not exceed 5-15 wt% (Burnham, 1967; London et al., 1988; Webster and Holloway, 1988). However, several observations indicate that these solubilities, and thus the potential for MVP to transport and deposit silicate components, may be higher than these estimates. So far, most experimental and thermodynamic studies on elemental solubilities in magmatic fluids focus on comparably simple systems, such as element and mineral solubilities in fluids in equilibrium with a single mineral phase as a function of pressure, temperature and salinity (Antignano and Manning, 2008; Dolejš and Manning, 2010; Rapp et al., 2010; Mair et al., 2017; Brooks and Steele-MacInnis, 2019). As mineral solubilities commonly depend on other solutes, particularly those of flux elements (see section 2.3), there is growing consensus that mineral (and melt) solubilities increase significantly the more complexly buffered a fluid is (Hayden and Manning, 2011; Mysen, 2019). At the extreme of the solubility spectrum, complete miscibility between MVP and melt has been considered to be mostly relevant for higher-pressure mantle systems (Bureau and Keppler, 1999). For shallow silicic systems, such miscibility has also been demonstrated by experiments in the peralkaline Fsp-Qtz-H_2O system (Mustart, 1972; Lundstrom, 2016; Lundstrom, 2020) and by inclusions in pegmatitic quartz (Webster et al., 1997; Thomas and Davidson, 2016; Thomas et al., 2019). These inclusions are particularly intriguing as their compositions imply that granite-buffered high-temperature fluids contain major element solutes in similar proportions as present in the melt. This is key, as the granitic melt-like bulk composition of pegmatites has commonly been cited as the main reason to exclude a fluid-derived origin.

Nonetheless, it remains unclear how ubiquitous such near-critical fluids or single-phase hydrous silicate liquids are in shallow upper-crustal silicic systems. Preliminary assessments from melt and fluid inclusions in co-erupted granitic clasts suggest a limited role for such intermediate-density liquids, at least in subduction zone (I-type) magmatism (Fiedrich et al., 2020a; Fiedrich et al., 2020b). It also remains unclear how melt compositions can evolve to be sufficiently enriched in flux elements, without saturation of flux element-bearing minerals such as topaz, fluorite and Li-phases buffering the enrichment of these elements and thus preventing the continuous transition between silicate melt and solute-rich aqueous fluid (Dolejš and Baker, 2007). While in the context of long-lived mushy granitic source reservoirs, formation of pegmatites seems more likely to occur from volumetrically dominant solute-rich MVP rather than limited volumes of melt, future research will have to unveil how common near-critical solubilities or even true miscibility are in these systems.

5.4 Giant crystal growth and physical transport

If near-solidus silicic mushy magmatic systems are more likely to produce large volumes of solute-rich or even supercritical MVP, how could these liquids produce the famously coarse crystal sizes and typical zoned pegmatite textures? As numerous cooling rate experiments have demonstrated, disequilibrium crystallization as a result of undercooling is crucial in producing these textures (Fenn, 1986; Lentz and Fowler, 1992; London, 2009; Nabelek et al., 2010; London, 2014; Maneta and Baker, 2014; Sirbescu et al., 2017). Extraction from the reservoir and injection into host rock in the upper crust would lead to a pressure drop and rapidly expose near-critical solute-rich MVP to a colder-temperature environment (<300-400 °C). The decrease in temperature and pressure would result in a drastic drop in mineral solubilities in solute-rich MVP (Fig. 3B left leg of the miscibility curve; London et al. (1988)). In the case of a single-phase hydrous silicate liquid, it would move from the single-liquid field in Fig. 3B into the two-liquid field. In both cases, this process could drive strong supersaturation and rapid precipitation of minerals from this fluid or liquid. Precipitation of minerals along such a P-T-gradient could explain the commonly observed trend of increasing fractionation with distance from the source pluton (Page, 1953; London, 2014), which is difficult to explain with melt-dominated pegmatite models (Simmons and Webber, 2008; London and Morgan, 2012). Upon further precipitation, cooling and/or decompression, the fluid itself may separate into vapor and brine depending on its salinity (Veksler et al., 2002; Audétat and Edmonds, 2020), which is again associated with strong element fractionation and enrichment (Ashworth et al., 2018). During precipitation, the order of crystallizing minerals is controlled by their chemical potential, with the phase of the highest chemical potential crystallizing first (London, 2014). The resulting disequilibrium crystallization would promote (1) the formation of graphic granite, (2) the growth of large crystals, often with skeletal shapes, and (3) the typical pegmatite zoning with monomineralic layers observed in many settings. These textural features occur not only in petrographically late-stage assemblages, but in minerals formed throughout the crystallization sequences of most pegmatites (and sometimes other rocks, hence the wide use of the term “pegmatitic” (section 2.1)), suggesting that the circumstances that promote such disequilibria are an automatic consequence of the shared compositional and thermal regimes involved. Most dynamic crystallization experiments so far have been conducted on hydrous granitic melts (e.g. Fenn, 1986; London, 2009; Maneta and Baker, 2014; Sirbescu et al., 2017 and many others). However, similar processes are expected to control crystallization textures during precipitation from solute-rich MVP, and trace element abundances in pegmatitic quartz have been linked to kinetic crystallization at turbulent, high-Reynolds number conditions (Phelps et al., 2020), characteristics for low-viscosity fluids.

Formation of pegmatites from solute-rich MVP would also explain their occurrence not just as large bodies, but more commonly as cm- to dm-thick veinlets (e.g. Fig. 2C, D). Transport of rhyolitic melt at

typical water concentrations of 4-6 wt% through such small spaces would be made impossible by the extremely high viscosities of rhyolitic melts (10^3-10^5 Pa s at 700 °C and 6-12 wt% H_2O (Whittington et al., 2009)). Piling up of water and flux elements in mineral boundary layers during rapid crystallization will decrease viscosity locally (London, 2014), but is unlikely to affect the viscosity of the bulk liquid. Since pegmatites are usually inferred to have crystallized in situ and lack porphyritic textures akin to silicate melts containing previously crystallized phenocrysts (see description in Philpotts and Ague, 2009), transport to the place of deposition would have to occur prior to any extensive crystallization, which would be required to modify melt viscosities sufficiently in the case of pegmatite formation from silicate melt (section 2.2).

This transport problem diminishes when considering solute-rich MVP or a single-phase liquid as the pegmatite-forming medium. Experiments in the albite-H_2O system suggest that within addition of <20 wt% H_2O, viscosities of miscible water-silicate melt mixtures decrease drastically compared to those of highly viscous silicate melts (Audétat and Keppler 2004, Hack and Thompson 2011), and are only slightly higher than those of aqueous fluids when containing >30 wt% H_2O. Based on a compilation of inclusion data for supercritical liquid entrapped in quartz from five different pegmatite systems, Thomas and Davidson (2015) propose a H_2O concentration of 26.5±1.5 wt% in the pegmatite-forming liquid. If viscosities in the silicate melt-H_2O system follow a similar trend as in the albite-H_2O system (Audétat and Keppler 2004), a single-phase liquid at these water contents would have a viscosity 4 orders of magnitude lower than that of anhydrous melt, and 3 orders of magnitude higher than that of pure H_2O. These intermediate viscosities would facilitate elemental transport and extraction of these liquids from their sources, but may limit diffusivities sufficiently to allow coarsening of crystal sizes through constitutional zone refining and the development of monomineralic layering during rapid precipitation (London, 2009; London, 2014).

6. Implications

Pegmatites are the last drops of magmatic distillates that are expelled at the end of the crystallization sequence of magmatic reservoirs. At near-solidus conditions, magmatic reservoirs are volumetrically dominated by MVP and crystals rather than melt, suggesting that pegmatites may be more likely to form from solute-rich MVP that is released from the reservoir into the surrounding cooler country rock via episodic hydraulic fracturing. Many of the textural and mineralogical aspects of pegmatites can be explained by progressive precipitation of minerals from complexly enriched MVP as the system cools. Such pegmatitic liquids may consist of solute-rich MVP or even single-phase hydrous silicate liquids, similar to those long recognized in high-pressure systems and playing a key role in element transport

during subduction, mantle metasomatism and melting (Tatsumi et al., 1986; Poli and Schmidt, 1995; Tatsumi and Eggins, 1995; Manning, 2004; Hacker, 2008; Galvez et al., 2016).

A holistic view of the plutonic, volcanic and pegmatitic realms can be achieved within the recent concept of crustal-scale magmatic plumbing systems (Bachmann and Huber, 2016; Cashman et al., 2017), providing an integrative concept for various magmatic products (Fig. 6). Evidence of all three realms can even be found in single (volcanic) units, as for example documented by plutonic fragments and U-rich pegmatite-like zircon domains in rhyolites from the Yellowstone region (Ellis et al., 2014; Troch et al., 2017; Troch et al., 2018). Coarse-grained, quartz-rich segregations (Fig. 2C and D) and interstitial quartz with low Ti contents (<20-30 ppm) occur in many plutonic units around the world (Ackerson et al., 2015; Ackerson et al., 2018; Fiedrich et al., 2020a; Rottier and Casanova, 2020), and may also have crystallized from such late trapped pegmatitic fluids. Although additional experiments and studies on natural systems are required to fully understand the physical and chemical behavior of such complexly enriched liquids in the upper crust, we encourage the research community to view pegmatites/aplites, plutonic rocks and volcanic deposits not as discrete entities, but to treat them as aspects of a continuous igneous distillation system. Like a good rug, pegmatites really tie the "magmatic room" together. As recorders of these late-stage enriched fluids, pegmatites are indeed the hallmark of the magmatic-hydrothermal transition.

Acknowledgements

We are deeply grateful to Jim Webster, who encouraged us to start venturing on this path. Noëmi Löw is thanked for her help in compiling partitioning and diffusion data for this paper. We also thank Julien Allaz, Matthieu Galvez, Ben Ellis, Alina Fiedrich, Nico Kueter and Paul Nex for enlightening discussions on the topic, and the Coen brothers as a source of inspiration. We are grateful for the thorough and helpful reviews by Paul Tomascak, David London, Peter Nabelek, Alex Iverson, Craig Lundstrom and an anonymous reviewer, and thank Dan Harlov and Don Baker for the editorial handling. OB and JT were supported by SNSF grant # 200021_178928 during the writing of this paper. CH was supported by NSF grant 1760004.

References

Ackerson, M.R., Mysen, B., Tailby, N., and Watson, E. (2018) Low-temperature crystallization of granites and the implications for crustal magmatism. Nature, 1.

627 Ackerson, M.R., Tailby, N.D., and Watson, E.B. (2015) Trace elements in quartz shed light on sediment provenance.
628 Geochemistry, Geophysics, Geosystems, 16(6), 1894-1904.
629 Anderson, A.T.J., Swihart, G.H., Artioli, G., and Geiger, C.A. (1984) Segregation Vesicles, Gas Filter-Pressing, and Igneous
630 Differentiation. The Journal of Geology, 92(1), 55-72.
631 Anderson, J.L. (2012) Cold pegmatites. Elements, 8, 248-249.
632 Antignano, A., and Manning, C.E. (2008) Fluorapatite solubility in H2O and H2O–NaCl at 700 to 900 C and 0.7 to 2.0 GPa.
633 Chemical Geology, 251(1-4), 112-119.
634 Ashworth, L., Kinnaird, J., Nex, P., Harris, C., and Müller, A. (2020) Origin of rare-element-mineralized Damara Belt
635 pegmatites: A geochemical and light stable isotope study. Lithos, 372, 105655.
636 Ashworth, L., Kinnaird, J.A., Nex, P.A.M., Erasmus, R.M., and Przybyłowicz, W.J. (2018) Characterization of fluid inclusions
637 from mineralized pegmatites of the Damara Belt, Namibia: insight into late-stage fluid evolution and implications for
638 mineralization. Mineralogy and Petrology, 112(6), 753-765.
639 Audétat, A., and Edmonds, M. (2020) Magmatic-Hydrothermal Fluids. Elements: An International Magazine of Mineralogy,
640 Geochemistry, and Petrology, 16(6), 401-406.
641 Austin, G.S. (1994) Pumice mining and environmental concerns in New Mexico. New Mexico Geology, 16(1), 1-6.
642 Bachmann, O., and Bergantz, G.W. (2004) On the origin of crystal-poor rhyolites: extracted from batholithic crystal mushes.
643 Journal of Petrology, 45(8), 1565-1582.
644 Bachmann, O., and Huber, C. (2016) Silicic magma reservoirs in the Earth's crust. American Mineralogist, 101(11), 2377-2404.
645 -. (2018) The Inner Workings of Crustal Distillation Columns; the Physical Mechanisms and Rates Controlling Phase Separation
646 in Silicic Magma Reservoirs. Journal of Petrology, 60(1), 3-18.
647 Bachmann, O., Miller, C.F., and de Silva, S.L. (2007) The volcanic–plutonic connection as a stage for understanding crustal
648 magmatism. Journal of Volcanology and Geothermal Research, 167(1-4), 1-23.
649 Bai, T., and van Groos, A.K. (1994) Diffusion of chlorine in granitic melts. Geochimica et Cosmochimica Acta, 58(1), 113-123.
650 Bartels, A., Behrens, H., Holtz, F., Schmidt, B.C., Fechtelkord, M., Knipping, J., Crede, L., Baasner, A., and Pukallus, N. (2013)
651 The effect of fluorine, boron and phosphorus on the viscosity of pegmatite forming melts. Chemical Geology, 346,
652 184-198.
653 Bartels, A., Vetere, F., Holtz, F., Behrens, H., and Linnen, R.L. (2011) Viscosity of flux-rich pegmatitic melts. Contributions to
654 Mineralogy and Petrology, 162(1), 51-60.
655 Barth, T.W. (1939) Die Eruptivgesteine. In C.W. Correns, Ed. Die Entstehung der Gesteine, p. 97-100. Julius Springer Verlag,
656 Berlin.
657 Bartoli, O., Cesare, B., Poli, S., Bodnar, R.J., Acosta-Vigil, A., Frezzotti, M.L., and Meli, S. (2013) Recovering the composition
658 of melt and the fluid regime at the onset of crustal anatexis and S-type granite formation. Geology, 41(2), 115-118.
659 Bea, F., Pereira, M., and Stroh, A. (1994) Mineral/leucosome trace-element partitioning in a peraluminous migmatite (a laser
660 ablation-ICP-MS study). Chemical Geology, 117(1-4), 291-312.
661 Beard, J.S., and Day, H.W. (1986) Origin of gabbro pegmatite in the Smartville intrusive complex, northern Sierra Nevada,
662 California. American Mineralogist, 71(9-10), 1085-1099.
663 Bercovici, D., Ricard, Y., and Schubert, G. (2001) A two-phase model for compaction and damage: 1. General theory. Journal of
664 Geophysical Research: Solid Earth, 106(B5), 8887-8906.
665 Bindeman, I.N., and Davis, A.M. (2000) Trace element partitioning between plagioclase and melt: investigation of dopant
666 influence on partition behavior. Geochimica et Cosmochimica Acta, 64(16), 2863-2878.
667 Bindeman, I.N., Davis, A.M., and Drake, M.J. (1998) Ion microprobe study of plagioclase-basalt partition experiments at natural
668 concentration levels of trace elements. Geochimica et Cosmochimica Acta, 62(7), 1175-1193.
669 Brisbin, W.C. (1986) Mechanics of pegmatite intrusion. American Mineralogist, 71(3-4), 644-651.
670 Brooks, H.L., and Steele-MacInnis, M. (2019) A model for the solubility of minerals in saline aqueous fluids in the crust and
671 upper mantle. American Journal of Science, 319(9), 754-787.
672 Bureau, H., and Keppler, H. (1999) Complete miscibility between silicate melts and hydrous fluids in the upper mantle:
673 experimental evidence and geochemical implications. Earth and Planetary Science Letters, 165(2), 187-196.
674 Burnham, C.W. (1967) Hydrothermal fluids at the magmatic stage. In H.L. Barnes, Ed. Geochemistry of hydrothermal ore
675 deposits, p. 34-76.
676 Burnham, C.W., and Jahns, R.H. (1962) A method for determining the solubility of water in silicate melts. American Journal of
677 Science, 260(10), 721-745.
678 Cameron, E.N., Jahns, R.H., McNair, A.H., and Page, L.R. (1949) Internal structure of granitic pegmatites. Econ. Geol.,
679 Monograph, 2, 115.
680 Candela, P.A. (1994) Combined chemical and physical model for plutonic devolatilization: A non-Rayleigh fractionation
681 algorithm. Geochimica et Cosmochimica Acta, 58(10), 2157-2167.
682 -. (1997) A Review of Shallow, Ore-related Granites: Textures, Volatiles, and Ore Metals. Journal of Petrology, 38(12), 1619-
683 1633.
684 Cashman, K.V., Sparks, R.S.J., and Blundy, J.D. (2017) Vertically extensive and unstable magmatic systems: a unified view of
685 igneous processes. Science, 355(6331), eaag3055.

Cassidy, M., Manga, M., Cashman, K., and Bachmann, O. (2018) Controls on explosive-effusive volcanic eruption styles. Nature communications, 9(1), 2839.

Černý, P. (1991a) Rare-element Granitic Pegmatites. Part I: Anatomy and Internal Evolution of Pegmatitic Deposits. Geoscience Canada, 18(2).

-. (1991b) Rare-element Granitic Pegmatites. Part II: Regional to Global Environments and Petrogenesis. Geoscience Canada, 18(2).

Černý, P., Blevin, P., Cuney, M., and London, D. (2005) Granite-related Ore Deposits. Economic Geology, 100th Anniversary Volume.

Černý, P., London, D., and Novák, M. (2012) Granitic Pegmatites as Reflections of Their Sources. Elements, 8(4), 289-294.

Chakoumakos, B.C., and Lumpkin, G.R. (1990) Pressure-temperature constraints on the crystallisation of the Harding Pegmatite, Taos County, New Mexico. Canadian Mineralogist, 28, 287-298.

Cloos, M. (2001) Bubbling Magma Chambers, Cupolas, and Porphyry Copper Deposits. International Geology Review, 43(4), 285-311.

Connolly, J.A.D. (2010) The Mechanics of Metamorphic Fluid Expulsion. Elements, 6(3), 165-172.

Cooper, K.M., and Kent, A.J. (2014) Rapid remobilization of magmatic crystals kept in cold storage. Nature.

Davidovits, J. (1991) Geopolymers: Inorganic polymeric new materials. Journal of Thermal Analysis and Calorimetry, 37(8), 1633-1656.

Deering, C., and Bachmann, O. (2010) Trace element indicators of crystal accumulation in silicic igneous rocks. Earth and Planetary Science Letters, 297(1-2), 324-331.

Degruyter, W., Huber, C., Bachmann, O., Cooper, K.M., and Kent, A.J.R. (2017) Influence of Exsolved Volatiles on Reheating Silicic Magmas by Recharge and Consequences for Eruptive Style at Volcan Quizapu (Chile). Geochemistry, Geophysics, Geosystems, 18(11), 4123-4135.

Degruyter, W., Parmigiani, A., Huber, C., and Bachmann, O. (2019) How do volatiles escape their shallow magmatic hearth? Philosophical Transactions of the Royal Society A, 377(2139), 20180017.

Dill, H.G. (2015) Pegmatites and aplites: Their genetic and applied ore geology. Ore Geology Reviews, 69, 417-561.

Dingwell, D.B., Harris, D.M., and Scarfe, C.M. (1984) The solubility of H2O in melts in the system SiO2-Al2O3-Na2O-K2O at 1 to 2 kbars. The Journal of Geology, 92(4), 387-395.

Dolejš, D., and Baker, D.R. (2007) Liquidus equilibria in the system K2O–Na2O–Al2O3–SiO2–F2O− 1–H2O to 100 MPa: II. Differentiation paths of fluorosilicic magmas in hydrous systems. Journal of Petrology, 48(4), 807-828.

Dolejš, D., and Manning, C. (2010) Thermodynamic model for mineral solubility in aqueous fluids: theory, calibration and application to model fluid-flow systems. Geofluids, 10(1-2), 20-40.

Dufek, J., and Bachmann, O. (2010) Quantum magmatism: Magmatic compositional gaps generated by melt-crystal dynamics. Geology, 38(8), 687-690.

Edmonds, M., and Wallace, P.J. (2017) Volatiles and exsolved vapor in volcanic systems. Elements, 13(1), 29-34.

Ellis, B.S., Bachmann, O., and Wolff, J.A. (2014) Cumulate fragments in silicic ignimbrites: The case of the Snake River Plain. Geology, 42(5), 431-434.

Fenn, P.M. (1986) On the origin of graphic granite. American Mineralogist, 71(3-4), 325-330.

Fiedrich, A.M., Heinrich, C.A., and Bachmann, O. (2020a) Evolution from magmatic to hydrothermal activity beneath the Cerro Escorial volcano (NW Argentina) as sampled by erupted quartz and brines. Lithos, 105706.

Fiedrich, A.M., Laurent, O., Heinrich, C.A., and Bachmann, O. (2020b) Melt and fluid evolution in an upper-crustal magma reservoir, preserved by inclusions in juvenile clasts from the Kos Plateau Tuff, Aegean Arc, Greece. Geochimica et Cosmochimica Acta.

Franz, H., and Scholze, H. (1963) The Solubility of Water Vapor in Glass Melts of Different Basicity. Glastech. Ber, 36(9), 347-356.

Frezzotti, M.L. (1992) Magmatic immiscibility and fluid phase evolution in the Mount Genis granite (southeastern Sardinia, Italy). Geochimica et Cosmochimica Acta, 56(1), 21-33.

Fuchsloch, W.C., Nex, P.A., and Kinnaird, J.A. (2018) Classification, mineralogical and geochemical variations in pegmatites of the Cape Cross-Uis pegmatite belt, Namibia. Lithos, 296, 79-95.

Gabitov, R., Price, J., and Watson, E. (2005) Diffusion of Ca and F in haplogranitic melt from dissolving fluorite crystals at 900–1000 C and 100 MPa. Geochemistry, Geophysics, Geosystems, 6(3).

Galvez, M.E., Connolly, J.A., and Manning, C.E. (2016) Implications for metal and volatile cycles from the pH of subduction zone fluids. Nature, 539(7629), 420-424.

Giordano, D., Romano, C., Dingwell, D., Poe, B., and Behrens, H. (2004) The combined effects of water and fluorine on the viscosity of silicic magmas. Geochimica et Cosmochimica Acta, 68(24), 5159-5168.

Goodenough, K.M., Shaw, R.A., Smith, M., Estrade, G., Marqu, E., Bernard, C., and Nex, P. (2019) Economic mineralization in pegmatites: comparing and contrasting NYF and LCT examples. The Canadian Mineralogist, 57(5), 753-755.

Gysi, A.P., Williams-Jones, A.E., and Collins, P. (2016) Lithogeochemical vectors for hydrothermal processes in the Strange Lake peralkaline granitic REE-Zr-Nb deposit. Economic Geology, 111(5), 1241-1276.

Hacker, B.R. (2008) H2O subduction beyond arcs. Geochemistry, Geophysics, Geosystems, 9(3).

Hayden, L.A., and Manning, C.E. (2011) Rutile solubility in supercritical NaAlSi3O8–H2O fluids. Chemical Geology, 284(1-2), 74-81.

Hildreth, W. (2004) Volcanological perspectives on Long Valley, Mammoth Mountain, and Mono Craters: several contiguous but discrete systems. Journal of Volcanology and Geothermal Research, 136(3-4), 169-198.

Holtz, F., Pichavant, M., Barbey, P., and Johannes, W. (1992) Effects of H2O on liquidus phase relations in the haplogranite system at 2 and 5 kbar. American Mineralogist, 77(11-12), 1223-1241.

Holtzman, R., Szulczewski, M.L., and Juanes, R. (2012) Capillary fracturing in granular media. Physical review letters, 108(26), 264504.

Holycross, M., Watson, E., Richter, F., and Villeneuve, J. (2018) Diffusive fractionation of Li isotopes in wet, highly silicic melts. Geochemical Perspectives Letters, 6, 39-42.

Huang, W.-L., and Wyllie, P. (1981) Phase relationships of S-type granite with H2O to 35 kbar: Muscovite granite from Harney Peak, South Dakota. Journal of Geophysical Research: Solid Earth, 86(B11), 10515-10529.

Huber, C., Bachmann, O., and Manga, M. (2009) Homogenization processes in silicic magma chambers by stirring and mushification (latent heat buffering). Earth and Planetary Science Letters, 283(1), 38-47.

Huber, C., Bachmann, O., Vigneresse, J.L., Dufek, J., and Parmigiani, A. (2012) A physical model for metal extraction and transport in shallow magmatic systems. Geochemistry, Geophysics, Geosystems, 13(8).

Huber, C., and Parmigiani, A. (2018) A Physical Model for Three-Phase Compaction in Silicic Magma Reservoirs. Journal of Geophysical Research: Solid Earth, 123(4), 2685-2705.

Iveson, A.A., Webster, J.D., Rowe, M.C., and Neill, O.K. (2019) Fluid-melt trace-element partitioning behaviour between evolved melts and aqueous fluids: Experimental constraints on the magmatic-hydrothermal transport of metals. Chemical Geology, 516, 18-41.

Jackson, M., Blundy, J., and Sparks, R. (2018) Chemical differentiation, cold storage and remobilization of magma in the Earth's crust. Nature, 564(7736), 405-409.

Jahns, R.H., and Burnham, C.W. (1969) Experimental studies of pegmatite genesis: l. A model for the derivation and crystallization of granitic pegmatites. Economic Geology, 64(8), 843-864.

Jahns, R.H., and Tuttle, O.F. (1963) Layered pegmatite-aplite intrusives. Mineralogical Society of America Special Paper, 1, 78-92.

Johannes, W., and Holtz, F. (1996) Petrogenesis and experimental petrology of granitic rocks. 328 p. Springer, Berlin.

Kontak, D.J., and Kyser, T.K. (2009) Nature and origin of an LCT-suite pegmatite with late-stage sodium enrichment, Brazil Lake, Yarmouth County, Nova Scotia. II. Implications of stable isotopes (δ18O, δD) for magma source, internal crystallization and nature of sodium metasomatism. The Canadian Mineralogist, 47(4), 745-764.

Koyaguchi, T., and Kaneko, K. (1999) A two-stage thermal evolution model of magmas in continental crust. Journal of Petrology, 40(2), 241-254.

Lamy-Chappuis, B., Heinrich, C.A., Driesner, T., and Weis, P. (2020) Mechanisms and patterns of magmatic fluid transport in cooling hydrous intrusions. Earth and Planetary Science Letters, 535, 116111.

Laurent, O., Björnsen, J., Wotzlaw, J.-F., Bretscher, S., Silva, M.P., Moyen, J.-F., Ulmer, P., and Bachmann, O. (2020) Earth's earliest granitoids are crystal-rich magma reservoirs tapped by silicic eruptions. Nature Geoscience, 13(2), 163-169.

Lentz, D.R., and Fowler, A.D. (1992) A dynamic model for quartz-feldspar graphic intergrowths from granitic pegmatites in the southwestern Grenville Province. The Canadian Mineralogist, 30(3), 571-585.

Lierenfeld, M.B., Zajacz, Z., Bachmann, O., and Ulmer, P. (2018) Sulfur diffusion in dacitic melt at various oxidation states: Implications for volcanic degassing. Geochimica et Cosmochimica Acta, 226, 50-68.

Linnen, R.L., Van Lichtervelde, M., and Černý, P. (2012) Granitic pegmatites as sources of strategic metals. Elements, 8(4), 275-280.

Lipman, P.W. (1984) The roots of ash flow calderas in western North America: windows into the tops of granitic batholiths. Journal of Geophysical Research: Solid Earth, 89(B10), 8801-8841.

Liu, Y., Zhang, Y., and Behrens, H. (2005) Solubility of H2O in rhyolitic melts at low pressures and a new empirical model for mixed H2O–CO2 solubility in rhyolitic melts. Journal of Volcanology and Geothermal Research, 143(1-3), 219-235.

London, D. (1992) The application of experimental petrology to the genesis and crystallization of granitic pegmatites. The Canadian Mineralogist, 30(3), 499-540.

London, D. (2008) Pegmatites. Can. Mineral., 10, 347.

-. (2009) The origin of primary textures in granitic pegmatites. The Canadian Mineralogist, 47(4), 697-724.

-. (2014) A petrologic assessment of internal zonation in granitic pegmatites. Lithos, 184, 74-104.

-. (2018) Ore-forming processes within granitic pegmatites. Ore Geology Reviews, 101, 349-383.

London, D., Hervig, R.L., and Morgan, G.B. (1988) Melt-vapor solubilities and elemental partitioning in peraluminous granite-pegmatite systems: experimental results with Macusani glass at 200 MPa. Contributions to Mineralogy and Petrology, 99(3), 360-373.

London, D., and Kontak, D.J. (2012) Granitic pegmatites: scientific wonders and economic bonanzas. Elements, 8(4), 257-261.

London, D., and Morgan, G.B. (2012) The pegmatite puzzle. Elements, 8(4), 263-268.

Lundstrom, C. (2020) Continuously changing quartz-albite saturated melt compositions to 330° C with application to heat flow and geochemistry of the ocean crust. Journal of Geophysical Research: Solid Earth, 125(2), e2019JB017654.
Lundstrom, C.C. (2016) The role of thermal migration and low-temperature melt in granitoid formation: can granite form without rhyolitic melt? International Geology Review, 58(3), 371-388.
MacKenzie, K.J. (2006) What are these things called geopolymers? A physicochemical perspective. Advances in Ceramic Matrix Composites IX, 153, 173-186.
Mair, P., Tropper, P., Harlov, D.E., and Manning, C.E. (2017) The solubility of apatite in H2O, KCl-H2O, NaCl-H2O at 800 C and 1.0 GPa: Implications for REE mobility in high-grade saline brines. Chemical Geology, 470, 180-192.
Maneta, V., and Baker, D.R. (2014) Exploring the effect of lithium on pegmatitic textures: An experimental study. American Mineralogist, 99(7), 1383-1403.
Manning, C.E. (2004) The chemistry of subduction-zone fluids. Earth and Planetary Science Letters, 223(1-2), 1-16.
Marsh, B. (1981) On the crystallinity, probability of occurrence, and rheology of lava and magma. Contributions to Mineralogy and Petrology, 78(1), 85-98.
Marsh, B. (2004) A magmatic mush column rosetta stone: the McMurdo Dry Valleys of Antarctica. Eos, Transactions American Geophysical Union, 85(47), 497-502.
Mesko, M., Schader, P., and Shelby, J. (2002) Water solubility and diffusion in sodium silicate melts. Physics and chemistry of glasses, 43(6), 283-290.
Mesko, M., and Shelby, J. (2001) Water solubility and diffusion in alkali silicate melts. Physics and chemistry of glasses, 42(3), 173-178.
Morgan, G.B.V., and London, D. (1999) Crystallization of the Little Three layered pegmatite-aplite dike, Ramona District, California. Contributions to Mineralogy and Petrology, 136(4), 310-330.
Morton, D.M., Sheppard, J.B., Miller, F.K., and Lee, C.-T.A. (2018) Petrogenesis of the cogenetic Stewart pegmatite-aplite, Pala, California: Regional implications. Lithosphere, 11(1), 91-128.
Müller, A., Romer, R.L., and Pedersen, R.-B. (2017) The Sveconorwegian pegmatite province–thousands of pegmatites without parental granites. The Canadian Mineralogist, 55(2), 283-315.
Mungall, J.E. (2015) Physical controls of nucleation, growth and migration of vapor bubbles in partially molten cumulates. Layered intrusions, p. 331-377. Springer.
Mungall, J.E., Dingwell, D., and Chaussidon, M. (1999) Chemical diffusivities of 18 trace elements in granitoid melts. Geochimica et Cosmochimica Acta, 63(17), 2599-2610.
Mustart, D.A. (1972) Phase Relations in the Peralkaline Portion of the System Na2O-Al2O3-SiO2-H2O. Department of Geology, Stanford University.
Mysen, B. (2019) Aqueous fluids as transport medium at high pressure and temperature: Ti4+ solubility, solution mechanisms, and fluid composition. Chemical Geology, 505, 57-65.
Mysen, B.O. (2007) The solution behavior of H2O in peralkaline aluminosilicate melts at high pressure with implications for properties of hydrous melts. Geochimica et Cosmochimica Acta, 71(7), 1820-1834.
Mysen, B.O., Cody, G.D., and Smith, A. (2004) Solubility mechanisms of fluorine in peralkaline and meta-aluminous silicate glasses and in melts to magmatic temperatures. Geochimica et Cosmochimica Acta, 68(12), 2745-2769.
Nabelek, P.I., Whittington, A.G., and Sirbescu, M.-L.C. (2010) The role of H 2 O in rapid emplacement and crystallization of granite pegmatites: resolving the paradox of large crystals in highly undercooled melts. Contributions to Mineralogy and Petrology, 160(3), 313-325.
Nair, B., Zhao, Q., and Cooper, R. (2007) Geopolymer matrices with improved hydrothermal corrosion resistance for high-temperature applications. Journal of materials science, 42(9), 3083-3091.
Neukampf, J., Ellis, B.S., Magna, T., Laurent, O., and Bachmann, O. (2019) Partitioning and isotopic fractionation of lithium in mineral phases of hot, dry rhyolites: the case of the Mesa Falls Tuff, Yellowstone. Chemical Geology, 506, 175-186.
Newman, S., and Lowenstern, J.B. (2002) VolatileCalc: a silicate melt–H2O–CO2 solution model written in Visual Basic for excel. Computers & Geosciences, 28(5), 597-604.
Ni, H., Zhang, L., Xiong, X., Mao, Z., and Wang, J. (2017) Supercritical fluids at subduction zones: Evidence, formation condition, and physicochemical properties. Earth-Science Reviews, 167, 62-71.
Niggli, P. (1912) Die Gasmineralisatoren im Magma. I. Mitteilung. Zeitschrift für anorganische Chemie, 75(1), 161-188.
-. (1920) Die leichtflüchtigen Bestandteile im Magma. B. G. Teubner, Leipzig.
Noble, D.C., Vogel, T.A., Peterson, P.S., Landis, G.P., Grant, N.K., Jezek, P.A., and McKee, E.H. (1984) Rare-element–enriched, S-type ash-flow tuffs containing phenocrysts of muscovite, andalusite, and sillimanite, southeastern Peru. Geology, 12(1), 35-39.
Norton, J.J. (1966) Ternary diagrams of the quartz-feldspar content of pegmatites in Colorado. US Government Printing Office.
Oppenheimer, J., Rust, A.C., Cashman, K.V., and Sandnes, B. (2015) Gas migration regimes and outgassing in particle-rich suspensions. Frontiers in Physics, 3, 60.
Page, L.R. (1953) Pegmatite Investigations 1942-1945, Black Hills, South Dakota. USGS Professional Paper, 247, p. 228.
Papale, P., Moretti, R., and Barbato, D. (2006) The compositional dependence of the saturation surface of H2O+ CO2 fluids in silicate melts. Chemical Geology, 229(1-3), 78-95.
Parfitt, L., and Wilson, L. (2008) Fundamentals of physical volcanology. 233 p. Blackwell Publishing.

Parmigiani, A., Degruyter, W., Leclaire, S., Huber, C., and Bachmann, O. (2017) The mechanics of shallow magma reservoir outgassing. Geochemistry, Geophysics, Geosystems, 18(8), 2887-2905.

Parmigiani, A., Faroughi, S., Huber, C., Bachmann, O., and Su, Y. (2016) Bubble accumulation and its role in the evolution of magma reservoirs in the upper crust. Nature, 532(7600), 492-495.

Phelps, P.R., Lee, C.-T.A., and Morton, D.M. (2020) Episodes of fast crystal growth in pegmatites. Nature communications, 11(1), 1-10.

Philpotts, A., and Ague, J. (2009) Principles of igneous and metamorphic petrology. Cambridge University Press.

Pichavant, M. (1987) Effects of B and H2O on liquidus phase relations in the haplogranite system at l kbar. American Mineralogist, 72(11-12), 1056-1070.

Pichavant, M., Kontak, D.J., Herrera, J.V., and Clark, A.H. (1988) The Miocene-Pliocene Macusani volcanics, SE Peru. Contributions to Mineralogy and Petrology, 100(3), 300-324.

Pistone, M., Arzilli, F., Dobson, K.J., Cordonnier, B., Reusser, E., Ulmer, P., Marone, F., Whittington, A.G., Mancini, L., and Fife, J.L. (2015) Gas-driven filter pressing in magmas: Insights into in-situ melt segregation from crystal mushes. Geology, 43(8), 699-702.

Poli, S., and Schmidt, M.W. (1995) H2O transport and release in subduction zones: experimental constraints on basaltic and andesitic systems. Journal of Geophysical Research: Solid Earth, 100(B11), 22299-22314.

Popa, R.-G., Bachmann, O., Ellis, B.S., Degruyter, W., Tollan, P., and Kyriakopoulos, K. (2019) A connection between magma chamber processes and eruptive styles revealed at Nisyros-Yali volcano (Greece). Journal of Volcanology and Geothermal Research, 387, 106666.

Rapp, D., and Shelby, J. (2003) Water diffusion and solubility in soda-lime-silica melts. Physics and chemistry of glasses, 44(6), 393-400.

Rapp, J., Klemme, S., Butler, I., and Harley, S. (2010) Extremely high solubility of rutile in chloride and fluoride-bearing metamorphic fluids: An experimental investigation. Geology, 38(4), 323-326.

Rottier, B., and Casanova, V. (2020) Trace element composition of quartz from porphyry systems: a tracer of the mineralizing fluid evolution. Mineralium Deposita, 1-20.

Sánchez-Muñoz, L., Müller, A., Andrés, S.L., Martin, R.F., Modreski, P.J., and de Moura, O.J. (2017) The P–Fe diagram for K-feldspars: A preliminary approach in the discrimination of pegmatites. Lithos, 272, 116-127.

Scaillet, B., Clémente, B., Evans, B.W., and Pichavant, M. (1998) Redox control of sulfur degassing in silicic magmas. Journal of Geophysical Research: Solid Earth, 103(B10), 23937-23949.

Schaltegger, U., Ulianov, A., Müntener, O., Ovtcharova, M., Peytcheva, I., Vonlanthen, P., Vennemann, T., Antognini, M., and Girlanda, F. (2015) Megacrystic zircon with planar fractures in miaskite-type nepheline pegmatites formed at high pressures in the lower crust (Ivrea Zone, southern Alps, Switzerland). American Mineralogist, 100(1), 83-94.

Schilling, J.-G.E. (1966) Rare earth fractionation in Hawaiian volcanic rocks. Massachusetts Institute of Technology.

Shearer, C.K., Papike, J.J., and Jolliff, B.L. (1992) Petrogenetic links among granites and pegmatites in the Harney Peak rare-element granite-pegmatite system, Black Hills, South Dakota. The Canadian Mineralogist, 30(3), 785-809.

Shinohara, H., and Hedenquist, J. (1997) Constraints on magma degassing beneath the Far Southeast porphyry Cu–Au deposit, Philippines. Journal of Petrology, 38(12), 1741-1752.

Sillitoe, R.H. (2010) Porphyry copper systems. Economic geology, 105(1), 3-41.

Simmons, W.B.S., and Webber, K.L. (2008) Pegmatite genesis: state of the art. European Journal of Mineralogy, 20(4), 421-438.

Sirbescu, M.-L.C., and Nabelek, P.I. (2003) Crustal melts below 400 C. Geology, 31(8), 685-688.

Sirbescu, M.-L.C., Schmidt, C., Veksler, I.V., Whittington, A.G., and Wilke, M. (2017) Experimental crystallization of undercooled felsic liquids: generation of pegmatitic texture. Journal of Petrology, 58(3), 539-568.

Sisson, T.W., and Bacon, C.R. (1999) Gas-driven filter pressing in magmas. Geology, 27(7), 613-616.

Sowerby, J.R., and Keppler, H. (2002) The effect of fluorine, boron and excess sodium on the critical curve in the albite–H 2 O system. Contributions to Mineralogy and Petrology, 143(1), 32-37.

Stilling, A., Ćerný, P., and Vanstone, P.J. (2006) The Tanco pegmatite at Bernic Lake, Manitoba. XVI. Zonal and bulk compositions and their petrogenetic significance. The Canadian Mineralogist, 44(3), 599-623.

Tatsumi, Y., and Eggins, S. (1995) Subduction zone magmatism. 224 p. Wiley.

Tatsumi, Y., Hamilton, D., and Nesbitt, R. (1986) Chemical characteristics of fluid phase released from a subducted lithosphere and origin of arc magmas: evidence from high-pressure experiments and natural rocks. Journal of Volcanology and Geothermal Research, 29(1-4), 293-309.

Taylor, R.P., and Fallick, A.E. (1997) The evolution of fluorine-rich felsic magmas: source dichotomy, magmatic convergence and the origins of topaz granite. Terra Nova, 9(3), 105-108.

Thomas, R., and Davidson, P. (2012) Water in granite and pegmatite-forming melts. Ore Geology Reviews, 46, 32-46.

Thomas, R., and Davidson, P. (2013) The missing link between granites and granitic pegmatites. Journal of Geosciences, 58(2), 183-200.

Thomas, R., and Davidson, P. (2016) Revisiting complete miscibility between silicate melts and hydrous fluids, and the extreme enrichment of some elements in the supercritical state—consequences for the formation of pegmatites and ore deposits. Ore Geology Reviews, 72, 1088-1101.

Thomas, R., Davidson, P., and Appel, K. (2019) The enhanced element enrichment in the supercritical states of granite–pegmatite systems. Acta Geochimica, 38(3), 335-349.

Thomas, R., Davidson, P., and Badanina, E. (2012) Water-and boron-rich melt inclusions in quartz from the Malkhan pegmatite, Transbaikalia, Russia. Minerals, 2(4), 435-458.

Thomas, R., Webster, J., and Heinrich, W. (2000) Melt inclusions in pegmatite quartz: complete miscibility between silicate melts and hydrous fluids at low pressure. Contributions to Mineralogy and Petrology, 139(4), 394-401.

Thomas, R., Webster, J.D., and Davidson, P. (2006) Understanding pegmatite formation: the melt and fluid inclusion approach. Melt inclusions in plutonic rocks, 36, 189-210.

Townsend, M., Huber, C., Degruyter, W., and Bachmann, O. (2019) Magma chamber growth during intercaldera periods: Insights from thermo-mechanical modeling with applications to Laguna del Maule, Campi Flegrei, Santorini, and Aso. Geochemistry, Geophysics, Geosystems, 20(3), 1574-1591.

Troch, J., Ellis, B.S., Mark, D.F., Bindeman, I.N., Kent, A.J.R., Guillong, M., and Bachmann, O. (2017) Rhyolite generation prior to a Yellowstone supereruption: Insights from the Island Park-Mount Jackson rhyolite series. Journal of Petrology, 0(0), 1-24.

Troch, J., Ellis, B.S., Schmitt, A.K., Bouvier, A.-S., and Bachmann, O. (2018) The dark side of zircon: textural, age, oxygen isotopic and trace element evidence of fluid saturation in the subvolcanic reservoir of the Island Park-Mount Jackson Rhyolite, Yellowstone (USA). Contributions to Mineralogy and Petrology, 173(7), 54.

Troll, V.R., Carracedo, J.C., Jägerup, B., Streng, M., Barker, A.K., Deegan, F.M., Perez-Torrado, F., Rodriguez-Gonzalez, A., and Geiger, H. (2017) Volcanic particles in agriculture and gardening. Geology Today, 33(4), 148-154.

Trumbull, R., Krienitz, M.-S., Gottesmann, B., and Wiedenbeck, M. (2008) Chemical and boron-isotope variations in tourmalines from an S-type granite and its source rocks: the Erongo granite and tourmalinites in the Damara Belt, Namibia. Contributions to Mineralogy and Petrology, 155(1), 1-18.

Tuttle, O.F., and Bowen, N.L. (1958) Origin of granite in the light of experimental studies in the system, NaAlSi3O8-KAlSi308-SiO2-H2O. 153 p. Geological Society of America.

Veksler, I.V., Thomas, R., and Schmidt, C. (2002) Experimental evidence of three coexisting immiscible fluids in synthetic granitic pegmatite. American Mineralogist, 87(5-6), 775-779.

Vigneresse, J.L., Barbey, P., and Cuney, M. (1996) Rheological transitions during partial melting and crystallization with application to felsic magma segregation and transfer. Journal of Petrology, 37(6), 1579-1600.

Wallace, P.J., Anderson, A.T., and Davis, A.M. (1995) Quantification of pre-eruptive exsolved gas contents in silicic magmas. Nature, 377(6550), 612-616.

Watson, E.B. (1991) Diffusion of dissolved CO2 and Cl in hydrous silicic to intermediate magmas. Geochimica et Cosmochimica Acta, 55(7), 1897-1902.

-. (1994) Diffusion in volatile-bearing magmas. Reviews in Mineralogy and Geochemistry, 30(1), 371-411.

Webber, K.L., Simmons, W.B., Falster, A.U., and Foord, E.E. (1999) Cooling rates and crystallization dynamics of shallow level pegmatite-aplite dikes, San Diego County, California. American Mineralogist, 84(5-6), 708-717.

Webster, J., Holloway, J., and Hervig, R. (1989) Partitioning of lithophile trace elements between H_2O and H 2 O+ CO_2 fluids and topaz rhyolite melt. Economic Geology, 84(1), 116-134.

Webster, J.D., and Duffield, W.A. (1994) Extreme halogen abundances in tin-rich magma of the Taylor Creek Rhyolite, New Mexico. Economic Geology, 89(4), 840-850.

Webster, J.D., and Holloway, J.R. (1988) Experimental constraints on the partitioning of Cl between topaz rhyolite melt and H2O and H2O+ CO2 fluids: new implications for granitic differentiation and ore deposition. Geochimica et Cosmochimica Acta, 52(8), 2091-2105.

Webster, J.D., Iveson, A.A., Rowe, M.C., and Webster, P.M. (2020) Chlorine and felsic magma evolution: Modeling the behavior of an under-appreciated volatile component. Geochimica et Cosmochimica Acta, 271, 248-288.

Webster, J.D., and Rebbert, C.R. (1998) Experimental investigation of H 2 O and Cl− solubilities in F-enriched silicate liquids; implications for volatile saturation of topaz rhyolite magmas. Contributions to Mineralogy and Petrology, 132(2), 198-207.

Webster, J.D., Thomas, R., Rhede, D., Förster, H.-J., and Seltmann, R. (1997) Melt inclusions in quartz from an evolved peraluminous pegmatite: Geochemical evidence for strong tin enrichment in fluorine-rich and phosphorus-rich residual liquids. Geochimica et Cosmochimica Acta, 61(13), 2589-2604.

Whalen, J.B., Currie, K.L., and Chappell, B.W. (1987) A-type granites: geochemical characteristics, discrimination and petrogenesis. Contributions to mineralogy and petrology, 95(4), 407-419.

Whittington, A.G., Bouhifd, M.A., and Richet, P. (2009) Amorphous materials: Properties, structure, and durability: The viscosity of hydrous NaAlSi3O8 and granitic melts: Configurational entropy models. American Mineralogist, 94(1), 1-16.

Zajacz, Z., Halter, W.E., Pettke, T., and Guillong, M. (2008) Determination of fluid/melt partition coefficients by LA-ICPMS analysis of co-existing fluid and silicate melt inclusions: controls on element partitioning. Geochimica et Cosmochimica Acta, 72(8), 2169-2197.

980
981
982
983
984 **Figure captions**
985
986 **Fig. 1:** (A-C) Different modes of dominant MVP transport as function of crystal volume content; (D)
987 degassing efficiency for different initial reservoir volumes containing an initial 5.5 wt% H_2O based on
988 Parmigiani et al. (2017); (E) accumulation of water in melt and MVP during closed-system crystallization
989 of an anhydrous mineral assemblage, compared to water saturation threshold at 5-8 wt% H_2O relevant for
990 upper crustal pressures (blue bar in background). Bright blue bar on right indicates range of water
991 contents in pegmatitic melt inclusions in Thomas and Davidson (2016); (F) trace element enrichment for
992 elements of different incompatibility during closed-system equilibrium/batch crystallization. Gray area
993 marks range of enrichment for the same elements during fractional/Rayleigh crystallization. Note how
994 most enrichment both for water and incompatible trace element occurs at extremely high crystallinities, at
995 which MVP remains trapped in the crystal framework and can only be transported through hydraulic
996 fracturing.
997
998 **Fig. 2:** (A) watermelon tourmaline from the Otjua gem-pegmatite close to Karibib, Namibia, (B) late-
999 stage beryl-bearing pegmatite pockets in the Spitzkoppe granite, Namibia, (C) example of pegmatitic vein
1000 crosscutting more competent mafic sheet in the coastal Maine granites, USA, and (D) example of a
1001 pegmatitic vein in its host granite (from the Japan Geological Survey Museum in Tsukuba, Japan).
1002
1003 **Fig. 3:** Phase diagrams for the H_2O-silicate melt system, schematically displaying changes in the extent of
1004 immiscibility between H_2O-dominated fluid and hydrous silicate melt as a function of (A) melt
1005 composition, and (B) flux elements in the system (e.g. F, B, Cl, Li, P, Na). This addition of flux elements
1006 has a similar effect as an increase in pressure (Bureau and Keppler 199, Hack et al. 2007, Mysen 2014,
1007 Sowerby and Keppler 2002) and will decrease the size of the miscibility gap in the binary silicate-H_2O
1008 system. In this sub-system, the miscibility gap closes towards higher temperatures, however, translated to
1009 a differentiating natural system (A) the changing melt compositions result in increasing miscibility
1010 towards lower temperatures, with potential full retrograde miscibility in extreme cases. Note the
1011 decreasing solubility of silicate components in the MVP with decreasing temperature in (B).

Fig. 4: Results from Simulation A, simulating mechanical phase separation in a matrix-melt-MVP system. Profiles of crystallinity (A), MVP volume fraction (B) and MVP velocity (C) are shown for different time steps of continuing crystallization in a 20-m subsection of a water-saturated silicic mush.

Fig. 5: Trace element enrichment in melt at top of compacting mush column as simulated with TheDUDE model (Simulation B). Enrichment factors describe trace element accumulation due to MVP ascending from a more crystalline mush region relative to closed-system equilibrium crystallization as a function of (A) differences in porosity between top and bottom of mush section, (B) differences in pore volume fraction of MVP between top and bottom, and (C) the fraction of MVP added from the bottom to the top. Dotted lines mark values chosen for the calculation of enrichment in other diagrams, e.g. dotted line in A marks porosity contrast chosen for calculations in B and C.

Fig. 6: Integrated view of pegmatite formation in mush-dominated upper crustal magma reservoirs from pulses of exsolved Magmatic Volatile Phase (MVP) that is enriched in variable degrees in flux elements (as illustrated by the color coding of the MVP in the schematics) and other incompatible elements depending on the degree of differentiation and the type and composition of the source granitic reservoir (right-hand panels). Note that this illustration is not meant to imply that all pegmatite-forming A-type systems have necessarily produced volcanic (caldera-forming) eruptions or that caldera-forming eruptions only occur in A-type systems.

This is the peer-reviewed, final accepted version for American Mineralogist, published by the Mineralogical Society of America.
The published version is subject to change. Cite as Authors (Year) Title. American Mineralogist, in press.
DOI: https://doi.org/10.2138/am-2021-7915. http://www.minsocam.org/

Table 1: Parameters used in Simulation A

Symbol	Signification	Units	Value
c_1	Melt-matrix drag term	Pa s/m^2	$\mu_m \phi^2(1-S)^2/k_w(S)$
c_2	Melt-MVP drag term		$\mu_f \phi^2 S^2/k_{nw}(S)$
g	Acceleration - gravity	m/s^2	9.81
H	Mush thickness	m	20
K_0	Geometrical factor	-	Order of 1
K_0'	Geometrical factor	-	Order of 1
L_x	Latent heat of crystallization	J/kg	300,000 (Huber and Parmigiani, 2018)
L_f	Latent heat of exsolution	J/kg	600,000 (Huber and Parmigiani, 2018)
P_i	Pressure in phase i	Pa	200 MPa at the top
S	MVP pore volume fraction	-	0.15 (initial condition)
V_f	MVP velocity	m/s	
V_m	Melt velocity	m/s	
V_x	Matrix velocity	m/s	
Γ_f	Exsolution rate	kg/m^{3}s	Calculated
Γ_x	Crystallization rate	kg/m^{3}s	$5x10^{-7}$
ϕ	Porosity	-	0.45 (initial condition)
ρ_f	MVP density	kg/m^3	EOS from Huber et al. (2010)
ρ_m	Melt density	kg/m^3	2500
ρ_x	Crystal density	kg/m^3	2800
μ_f	MVP viscosity	Pa s	10^{-2}
μ_m	Melt viscosity	Pa s	10^4
μ_x	Crystal viscosity	Pa s	10^{12}

This is the peer-reviewed, final accepted version for American Mineralogist, published by the Mineralogical Society of America.
The published version is subject to change. Cite as Authors (Year) Title. American Mineralogist, in press.
DOI: https://doi.org/10.2138/am-2021-7915. http://www.minsocam.org/

Table 2: Fluid-melt and mineral-melt partition coefficients used in Simulation B (TheDUDE)

Element	Kd(fluid-melt)	Reference	Kd(phase-melt)	Phase*	Reference
Boron	**3**	**preferred value**	**0.05**	**bulk**	**preferred value**
	0.3 - 5.2	Fiedrich et al. 2020b	0.01 - 0.08	bulk	range
	2 - 16	Zajacz et al. 2008	no data	Qtz	
	0.1 - 7.1	Webster et al. 1989	0.06 – 0.27	Plag	Bindeman and Davis 2000
	1.0 - 2.3	London et al. 1988	0.06 – 0.90	Plag	Bindeman et al. 1998
	1.2	Hervig et al. 2002	no data	San	
	0.5 - 6.3	Schatz et al. 2004			
	1.3 - 1.8	Thomas et al. 2003			
Sulfur	**20**	**preferred value**	**0.01**	**bulk**	**preferred value**
	1	Scaillet et al. 1998	no data	Qtz	
	47	Keppler 2010	no data	Plag	
	270	Scaillet and MacDonald 2006	no data	San	
	18 - 108	Botcharnikov et al. 2004			
Chlorine	**10**	**preferred value**	**0.3**	**bulk**	**preferred value**
	9 - 12	Villemant and Boudon 1999	0.01 - 0.03	bulk	range
	0.4 - 9.3	Botcharnikov et al. 2004	no data	Qtz	
	3 - 36	Iveson et al. 2019	0.43 - 1.58	Plag	Bindeman et al. 1998
	0.8 - 87	Webster and Holloway 1990	0.001	Plag	Dalou et al. 2012
	7 - 240	Webster and Rebbert 1998	no data	San	
	16 - 115	Webster et al. 2009			
	4 - 55	Métrich and Rutherford 1992			
Fluorine	**0.3**	**preferred value**	**0.8**	**bulk**	**preferred value**
	<1	Villemant and Boudon 1999	0.04 - 1.63	bulk	range
	0.4 - 0.5	London et al. 1988	no data	Qtz	
	0.1 - 0.4	Webster 1990	0.33 - 4.88	Plag	Bindeman et al. 1998
	0.2 - 1.1	Webster and Holloway 1990	0.09	Plag	Dalou et al. 2012
	0.04 - 3.8	Borodulin et al. 2009	no data	San	
	0.3 - 0.9	Xiaolin et al. 1998			
Lithium	**2**	**preferred value**	**0.3**	**bulk**	**preferred value**
	1.0 - 2.6	Fiedrich et al. 2020b	0.15 - 0.51	bulk	range
	2 - 41	Zajacz et al. 2008	0.31 - 0.58	Qtz	Neukampf et al. 2019
	0.05 - 1.2	Iveson et al. 2019	0.11 - 0.67	Plag	Neukampf et al. 2019
	0.3 - 0.4	London et al. 1988	0.72	Plag	Bea et al. 1994
			0.03 - 0.28	San	Neukampf et al. 2019

* bulk refers to an approximate eutectic assemblage of 1/3 quartz (Qtz), 1/3 plagioclase (Plag), and 1/3 sanidine (San). Where no data is available, we take KD(phase-melt) to be close to zero. Note that most crystal-melt partitioning data is based on basaltic system, data for rhyolitic systems is only available for Li.

This is the peer-reviewed, final accepted version for American Mineralogist, published by the Mineralogical Society of America.
The published version is subject to change. Cite as Authors (Year) Title. American Mineralogist, in press.
DOI: https://doi.org/10.2138/am-2021-7915. http://www.minsocam.org/

Figure 1

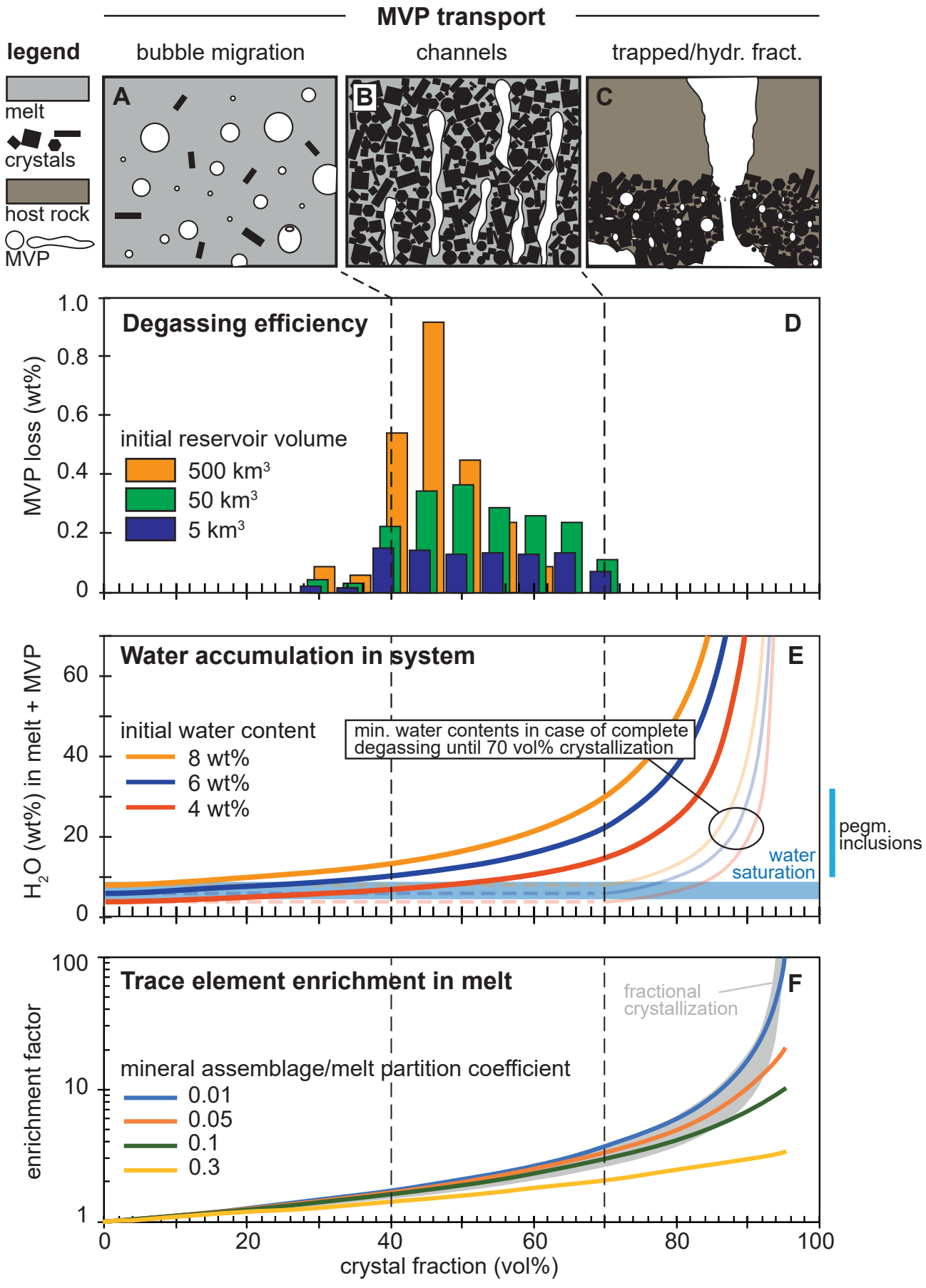

Figure 1

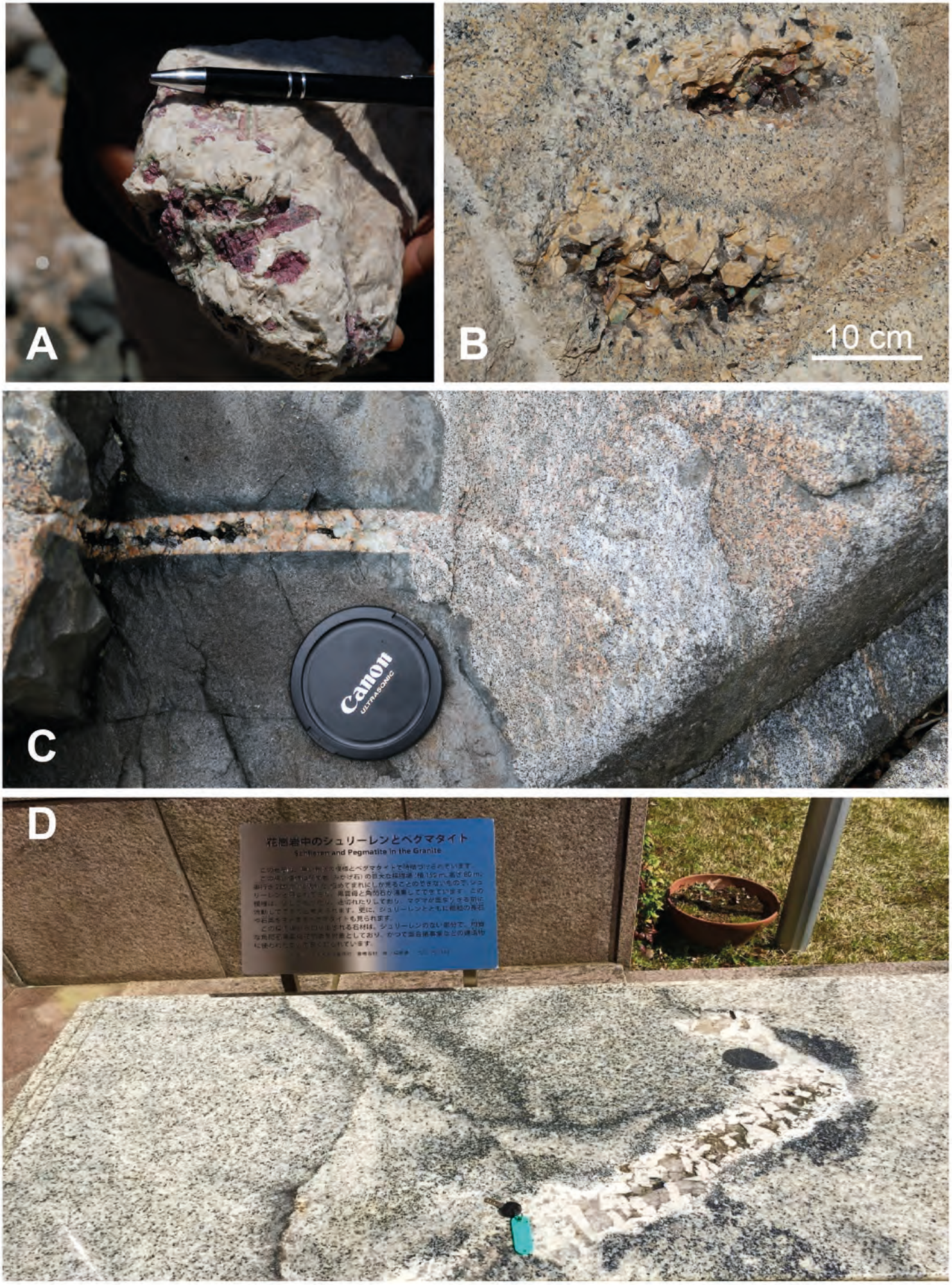

This is the peer-reviewed, final accepted version for American Mineralogist, published by the Mineralogical Society of America.
The published version is subject to change. Cite as Authors (Year) Title. American Mineralogist, in press.
DOI: https://doi.org/10.2138/am-2021-7915. http://www.minsocam.org/

Figure 3

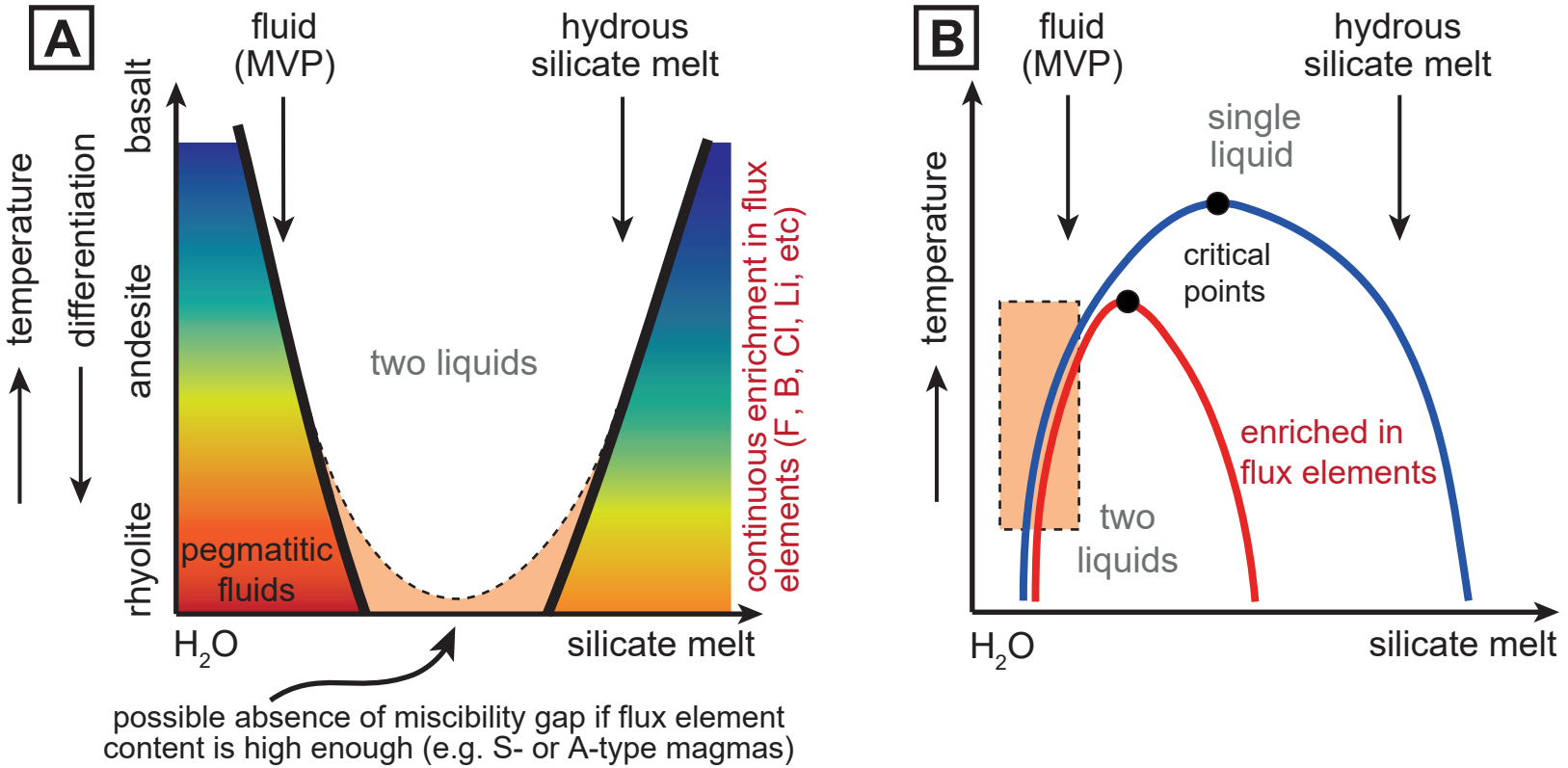

Figure 4

This is the peer-reviewed, final accepted version for American Mineralogist, published by the Mineralogical Society of America.
The published version is subject to change. Cite as Authors (Year) Title. American Mineralogist, in press.
DOI: https://doi.org/10.2138/am-2021-7915. http://www.minsocam.org/

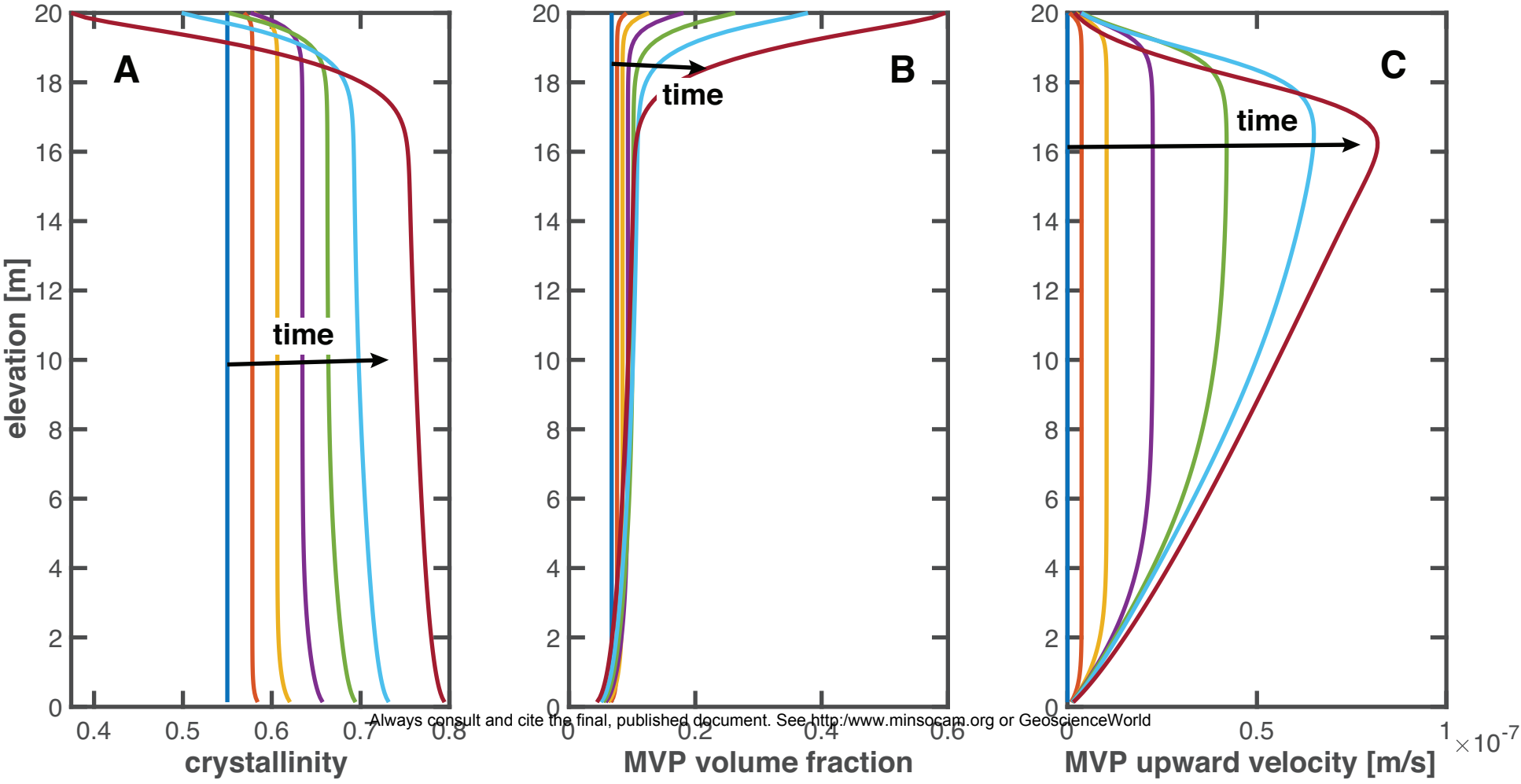

This is the peer-reviewed, final accepted version for American Mineralogist, published by the Mineralogical Society of America.
The published version is subject to change. Cite as Authors (Year) Title. American Mineralogist, in press.
DOI: https://doi.org/10.2138/am-2021-7915. http://www.minsocam.org/

Figure 5

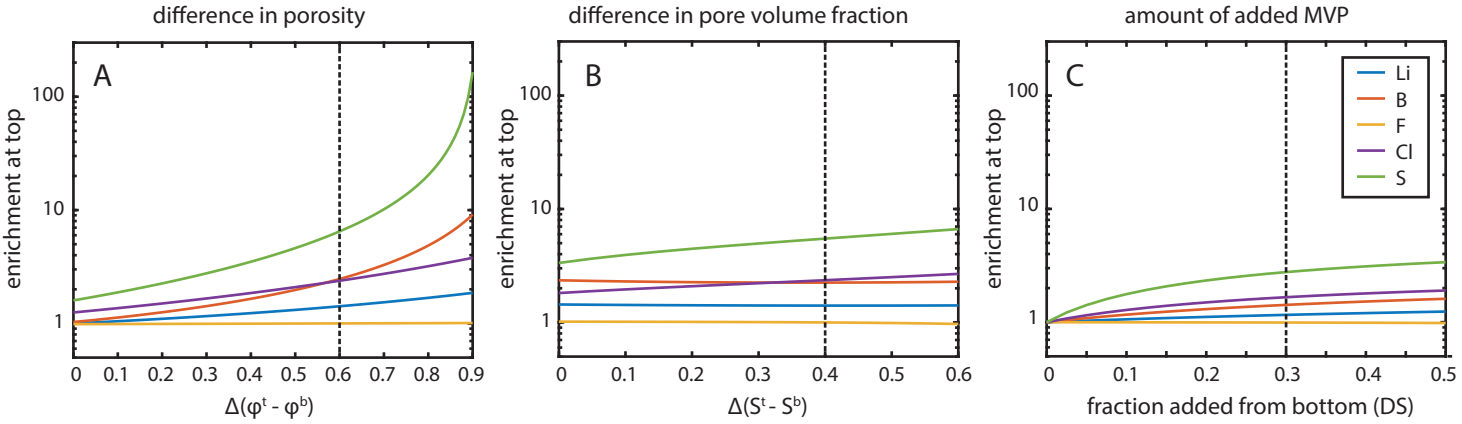

This is the peer-reviewed, final accepted version for American Mineralogist, published by the Mineralogical Society of America.
The published version is subject to change. Cite as Authors (Year) Title. American Mineralogist, in press.
DOI: https://doi.org/10.2138/am-2021-7915. http://www.minsocam.org/

Figure 6